

Review of Coreless Axial Flux Permanent Magnet Machines with Applications Including Electric Aircraft Propulsion

Matin Vatani, *Graduate Student Member, IEEE*, Donovan D. Lewis, *Graduate Student Member, IEEE*, John F. Eastham, *RAEng, Fellow*, and Dan M. Ionel, *Fellow, IEEE*

Abstract—Axial flux permanent magnet (AFPM) machines with entirely or stator coreless configurations offer significant advantages, including low rotational losses, the absence of cogging torque, minimal torque ripple, and the potential for high specific power density. Advances in permanent magnet (PM) technology and cooling techniques have enabled fully coreless AFPM machines to achieve high magnetic and current loadings without core saturation, making them suitable for high-performance applications like electric aircraft propulsion. This paper reviews recent advancements in coreless AFPM machines, tracing their historical and chronological development. Various topologies, including single- and double-sided and multi-disk designs, are examined to identify the advantages and emerging trends in each configuration. Different winding configurations are compared, and their performance characteristics are discussed. Recent innovations in winding materials, such as printed circuit boards (PCBs), are highlighted. The rotor configurations are reviewed, with a focus on the development of flux density equations and specific attention to Halbach array PM rotor due to its relevance for electric aircraft propulsion. The paper also discusses electromagnetic modeling techniques, including proposed analytical and 2D approaches that reduce the computational burden of traditional 3D calculations. Sources of power loss are identified, along with mitigation strategies based on existing literature. A preliminary design procedure and sizing evaluation are presented, utilizing analytical torque and back electromotive force (B-EMF) calculations through an equivalent 2D linear model. Finally, recent advancements in electric machines designed for aircraft propulsion are reviewed, showcasing their electromagnetic performance and highlighting the potential benefits of coreless machines in this field.

Index Terms—Review, axial flux PM machines, coreless stator, Halbach array, electric aircraft.

I. INTRODUCTION

Axial flux PM machines, characterized by an air-gap flux path perpendicular to the radial direction, present a compelling alternative to the more prevalent radial flux machines, which feature an air-gap flux parallel to the radial direction. These AFPM machines are particularly advantageous in applications requiring high torque density in a compact form factor with a short axial length relative to the outer diameter [1]–[3].

Matin Vatani, Donovan D. Lewis, and Dan M. Ionel are with SPARK Lab, Stanley and Karen Pigman College of Engineering, University of Kentucky, Lexington, KY, USA (e-mail: matin.vatani@uky.edu; donovin.lewis@uky.edu; dan.ionel@ieee.org).

John F. Eastham is with the Department of Electronic and Electrical Engineering, University of Bath, Claverton Down, Bath, BA2 7AY, UK (e-mail: jfeastham@aol.com).

Authors' manuscript version accepted for publication. The final published version is copyrighted by IEEE and will be available as: Vatani, M., Lewis, D. D., Eastham, J. F., and Ionel, D. M., "Review of Coreless Axial Flux Permanent Magnet Machines with Applications Including Electric Aircraft Propulsion", in IEEE Transactions on Transportation Electrification. ©2025 IEEE Copyright Notice. "Personal use of this material is permitted. Permission from IEEE must be obtained for all other uses, in any current or future media, including reprinting/republishing this material for advertising or promotional purposes, creating new collective works, for resale or redistribution to servers or lists, or reuse of any copyrighted component of this work in other works."

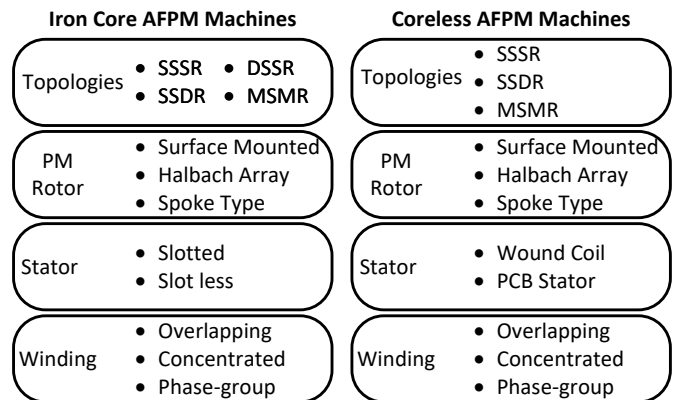


Fig. 1. Classifications for AFPM machines with and without the core. SSSR - single stator and single rotor; SSSR - single stator and double rotors; MSMR - multi-stators and multi rotors.

Axial flux PM machine designs and classifications vary significantly based on the construction and topological combination of rotors and stators. An example subset of classifications is shown in Fig. 1 between those that have a ferromagnetic core and those that do not. This paper focuses specifically on coreless AFPM machines and considers only designs operating at typical temperatures above ambient and does not include cryogenically cooled superconducting machines.

In coreless stator machines, the torque production mechanism can be explained based on the Lorentz force theorem, which involves the interaction between the rotor's rotating magnetic field and the current-carrying conductors [4]. Interest in coreless stator designs has grown in recent years due to their advantages in eliminating core-related losses, simplified construction, and the enablement of special cooling.

A typical example design and the main components of a coreless stator AFPM machines are illustrated in Fig. 2. In this case, the stator consists of a three-phase winding without any ferromagnetic material, while the rotor features PMs mounted on a back iron. The stator winding can be implemented with conventional stranded or Litz wire or in planar printed circuit boards (PCB), as demonstrated in [5], using copper traces encapsulated in FR4 laminate. Conventional wire-based windings are potted in a thermally conductive and electrically insulating epoxy. These potted coils are subsequently embedded into a non-ferromagnetic, electrically non-conductive plate, such as plastic, for improved structural stability, as exemplified in

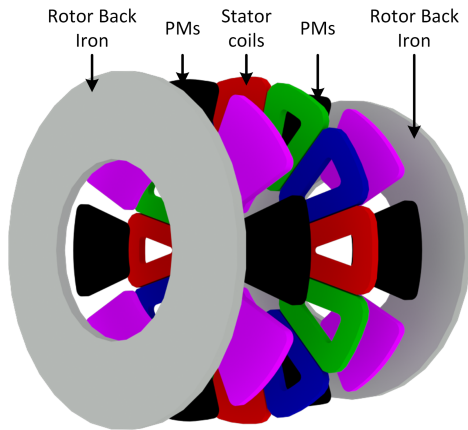


Fig. 2. Exploded view of an example double-sided eight pole, twelve coil axial flux permanent magnet (AFPM) machine with a coreless stator.

[5]. The surface-mounted rotor within the example design resembles that of the conventional AFPM machines, with magnets glued to a ferromagnetic disk.

The absence of steel material in the stator compared to its iron-cored counterparts offers several advantages. These machines exhibit significantly lower torque ripple, vibration, and noise due to the lack of ferromagnetic saliency, cogging, and reluctance torque. Additionally, ferromagnetic core losses, including eddy current and hysteresis components, are eliminated, allowing coreless AFPM machines to potentially achieve higher efficiencies than iron-cored alternatives [6], [7].

The absence of an iron core, which is the primary source of inductive reactance in conventional electric machines, significantly reduces reactive power components in coreless machines. Consequently, coreless AFPM machines have a low phase inductance and achieve a power factor close to unity [8]. This low phase inductance in these machines results in a high $\frac{dv}{dt}$, leading to increased current ripple. This issue can be effectively mitigated by employing higher switching frequencies, necessitating the use of Silicon Carbide (SiC) or Gallium Nitride (GaN) devices due to their low switching losses [9], [10].

Aircraft propulsion electrification replaces the thrust generated by traditional combustion engines with electric motors driving propellers. This transition demands electric propulsion systems with high power output, increased reliability, low mass, and high efficiency [11]. Ongoing projects in the United States aim to achieve a target specific power density exceeding 10 kW/kg for electric motor propulsion by leveraging advanced topologies and optimized thermal management systems. This goal marks a substantial advancement compared to the current world-record aviation motor, which achieves 5 kW/kg and was developed by Siemens [12].

Coreless stator machines offer the potential for high specific power density by eliminating the ferromagnetic core in the stator, which reduces mass and enables advanced cooling through improved access to all coil surfaces. These features, combined with low noise and vibration characteristics, make coreless stator machines suitable for aircraft propulsion systems. Axial flux implementation enhances these advantages

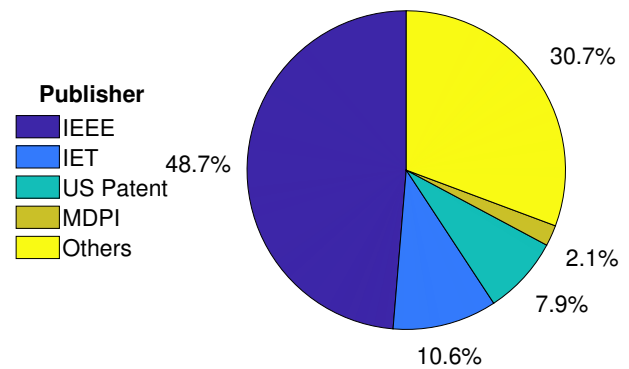


Fig. 3. Publisher distribution of the surveyed literature on coreless AFPM machines in this paper. Others in the figure include but are not limited to the reports and papers published by the Department of Energy, NASA, European patents, Springer, Elsevier, IOPscience, Taylor & Francis, and dissertations.

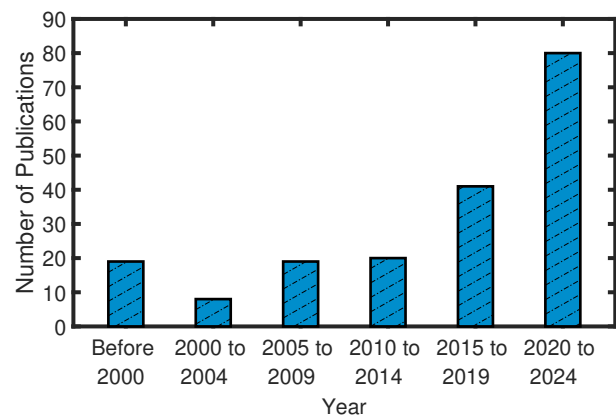


Fig. 4. Chronological distribution of the surveyed publications reviewed on coreless AFPM machines. Special attention was given to reviewing the state-of-the-art and recent developments.

by leveraging inherent benefits such as higher torque density and improved ability to achieve a modular design compared to conventional radial flux counterparts. For instance, multiple axial flux machines can be independently stacked along the axial direction, significantly improving fault tolerance and system reliability.

Previous review publications on AFPM machines, such as [13]–[15], have predominantly concentrated on iron-cored stators due to their more frequent development. In contrast, this paper considers coreless AFPM machine constructions and topologies. It provides a literature review of the latest electromagnetic modeling techniques and loss mitigation methods, tracing their development from a historical perspective.

The surveyed papers consider a wide range of applications, including but not limited to fans [17], [18], alternators and generators [17], [19], direct-drive wind turbines [20], [21], electric mobility [22], [23], and electric aircraft [24], [25]. Insights gained from literature on other applications are, in some instances, discussed in the context of their potential use in electric aircraft. As a result, this paper offers helpful information and can serve as a guideline for employing and designing coreless AFPM machines across various applications.

Some of the more common applications of coreless AFPM machines beyond aircraft propulsion and alternators include

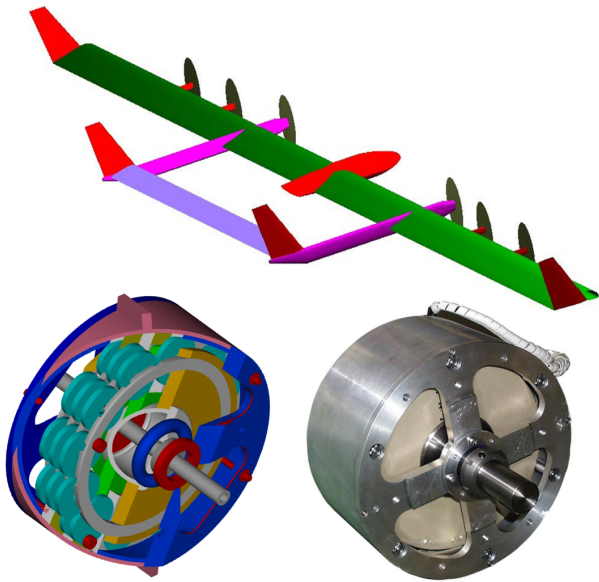


Fig. 5. Example aviation application including (a) stratospheric unmanned solar-powered aircraft concept designed in the early 2000s for border patrol and forest fire detection [16], (b) multi-disk coreless stator AFPM electric propulsion engine proposed by Eastham *et al.* [5], and (c) the prototyped machine.

HVAC systems, wind turbines, and marine turbines. For instance, coreless stator AFPM machines with PCB stators have been investigated for HVAC systems, demonstrating high efficiency enabled by automated and high-speed manufacturing processes [18], [26]. In the field of wind energy, these machines have been explored for direct-drive wind turbine generators due to their elimination of normal forces between the stator and rotors, which reduces mechanical complexity and the overall mass of the turbine system [20], [27]. Similarly, the advantages of lightweight structure and simplified mechanics have motivated the development of coreless AFPM generators for marine current turbine applications [28], [29].

The literature reviewed is in the form of papers, patents, and reports of which the authors had prior knowledge or were identified using a mixture of IEEExplore and Scopus, as illustrated in Fig. 3. The chronological distribution of the surveyed literature shown in Fig. 4, indicating significant increase in publications in the last decade, corresponding to major research efforts and advancements.

This review paper benefits from the historic and state-of-the-art perspectives of the two senior co-authors, who have followed and worked on the subject matter over the last three decades. Their groups' contributions span from the 90's work on the first European high-altitude unmanned aircraft [5], [16], [24], [30], [31], all the way to more recent US-based projects sponsored by industry, the National Science Foundation (NSF), and the National Aeronautics and Space Administration (NASA) for special EVs traction and electric propulsion [23], [25], [32]–[34].

The paper is structured in multiple sections, and following a brief historical perspective, including examples of significant developments over the years in Section II, main topologies with combinations of stators and rotors are discussed in

Section III. The stator windings, types, materials, and manufacturing technologies are reviewed in Section IV, followed by a similar discussion for rotors, including configurations and magnetization schemes in Section V. Electromagnetic modeling methods, which are key to machine design, are covered in Section VI, followed by a review of losses, components, and mitigation techniques in Section VII. The general sizing approach and equations for coreless AFPM machines are outlined in Section VIII and are followed by a comparative study of topologies and performance, including recent developments for electric aircraft propulsion.

II. BRIEF HISTORICAL PERSPECTIVE

Axial flux machines with coreless stators have been developed since the 1960s and have been described with terms ranging from “air-cored” to descriptors of the stator including, for example, “ironless,” “plastic,” and “non-ferromagnetic.” The first published mention of an axial flux machine of the coreless type was in 1963 by William Kober of The Garrett Corporation, Los Angeles, California, U.S., for an armature winding with “no associated ferromagnetic or other supporting structure” or “having no iron” [35]. In the early 1970s, the National Aeronautics and Space Administration (NASA) developed an “ironless” AFPM prototype using double-sided rotors with samarium-cobalt magnets and a coreless stator [36], [37]. In the 1980s and '90s, researchers at Imperial College, London, patented an axial flux machine with proposed variants including “multi-stranded coreless winding” within “rigid insulating substrate,” which spun off into Turbo Genset Co. Ltd. for commercialization [38], [39].

The coreless stator AFPM machines attracted more attention for various applications by the end of the 1990s as the PM industry developed more powerful magnets, especially with advances in rare earth PM production. In 1996/98, Caricchi *et al.* [40], [41] designed and prototyped a coreless stator AFPM generator with water-cooled and rhomboidal-shaped coils for ships, aircraft, or hybrid electric vehicle applications. In 1998, Mecrow *et al.* [42], [43] proposed and designed an in-wheel coreless stator AFPM machine with the Halbach array rotor for solar-powered vehicles. Lombard *et al.* [44] presented a design methodology for coreless stator AFPM machines using both lumped circuit modeling and finite element analysis in 1999. In the early 2000s, Eastham *et al.* [5], [24], [45] introduced a multi-stacked coreless stator AFPM motor for propeller-driven stratospheric aircraft, as demonstrated in Fig. 5.

With increased proposed applications of coreless axial flux machines, came attempts at commercialization by numerous companies. Some of the earliest patents found, other than Turbo Genset, include an “aircore” armature machine from Revolution Motor Company, Inc in 2005 [46], an axially stacked printed circuit board motor from Core Motion Inc. in 2006 [47], a machine with silicon steel supporting structure from Toshiba in 2007 [48], and a printed circuit board generator for wind turbine applications from Boulder Wind Power Inc. in 2011 [49]. Early commercially available motors include those from LaunchPoint Technologies for aerospace [50], [51] and Marand Precision Engineering for solar cars

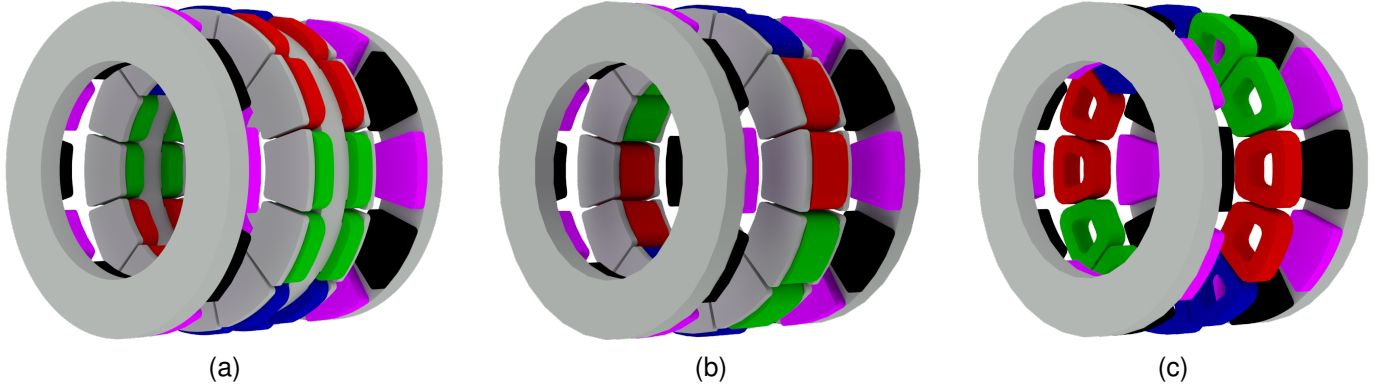


Fig. 6. Example AFPM machine topologies with (a) conventional yoked stator, (b) YASA yokeless and segmented armature stator, and (c) coreless stator.

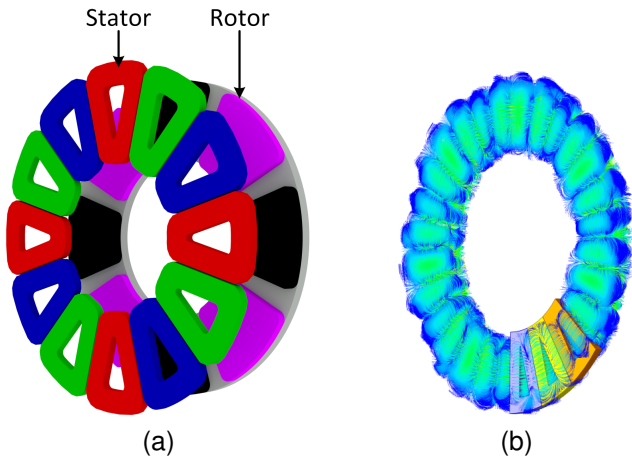


Fig. 7. An example single-stator single-rotor (SSSR) coreless stator AFPM machine (a) topology and (b) 3D flux distribution at no load calculated with 3D FEA. The rotor is of the surface-mounted PM type, and the stator has a single-layer, three-phase winding.

[22], [42], both of these used Halbach array magnetization. Options for commercial coreless stator AFPM machines are continually developing for a range of applications and sizes from companies, for example, such as E-Circuit Motors, Inc. [52] and Infinitum [17].

III. TOPOLOGIES

A coreless AFPM machine can be developed from traditional AFPM machines that utilize ferromagnetic materials in both the rotor and stator. The comparison of the coreless stator AFPM machine with a conventional AFPM machine and the yokeless and segmented armature (YASA) AFPM introduced by McCulloch *et al.* [53] is shown in Fig. 6. A conventional AFPM machine with a yoked stator structure is depicted in Fig. 6a. The YASA topology, which replaces the conventional yoked stator with a segmented stator, eliminating the stator back iron, is shown in Fig. 6b. A coreless stator AFPM machine, in which the segmented iron pieces in the coils of the YASA machine are removed, is illustrated in Fig. 6c.

The performance and cost comparison of conventional cored and coreless stator AFPM machines across multiple applications and power ratings is numerically analyzed and

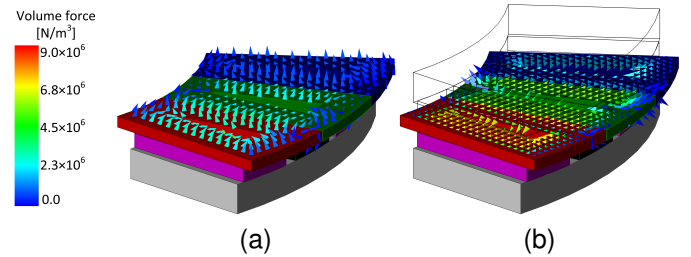


Fig. 8. Examples of force distribution of the stators on coreless machines in two configurations: (a) single-stator and single-rotor and (b) single-stator and double-rotor, illustrating that the use of two rotors minimizes the normal forces and variations.

discussed in [4]. The findings suggest that coreless AFPM machines are potentially lighter and more efficient, while conventional AFPM machines remain more cost-effective. Similarly, a study in [23] optimized and compared coreless and conventional AFPM machines for solar car propulsion. The results demonstrated that, given the same dimensions and current loading, the coreless AFPM machine is significantly lighter with reduced torque production compared to a cored variant. The reduced mass allows for the use of two coreless AFPM machines in a two-wheel drive configuration to meet the required torque while still being lighter than a conventional AFPM machine.

This section explores the topological variations in the surveyed literature for coreless AFPM machines. These topologies are categorized similarly to conventional AFPM machines based on the number of rotor and stator disks in their configurations [13], [15], [54]. Each topology is detailed, highlighting its unique features, along with a discussion of its advantages and limitations.

A. Single-Stator and Single-Rotor

The single-stator and single-rotor (SSSR) topology, shown in Fig. 7, represents the most fundamental form of a coreless stator AFPM machine, serving as the basis for more complex structures [1]. This topology consists of a stator with windings and a rotor featuring an iron disk on which PMs are mounted. Examples of employing this topology in the literature include the work by Neethu *et al.* [55], [56], which presented an SSSR

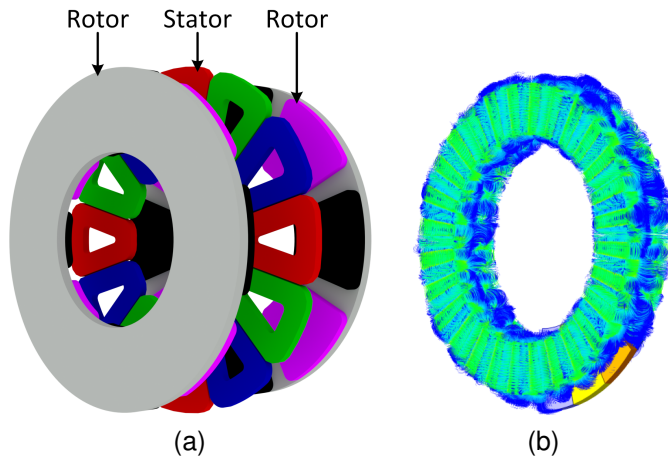


Fig. 9. An example single-stator double-rotor (SSDR) coreless stator AFPM machine (a) topology and (b) no load 3D flux distribution calculated via 3D FEA. This topology is the most typical structure employed in the surveyed literature.

coreless AFPM machine designed for high-speed, low-power applications, and the study by Barmatzta *et al.* [57], which compared the impact of PM demagnetization faults on the performance of SSSR and double-sided topologies.

In an SSSR, the flux encloses its path through the air to adjacent poles, whereas in a double-sided rotor configuration, the flux primarily crosses the air-gap in the normal direction. This difference results in SSSR having a higher tangential flux density component and a lower normal flux density component compared to the double-sided configuration. In coreless stator AFPM machines, torque generation is explained by the Lorentz force law, where the interaction between the rotor's magnetic flux density and the current density in the conductors produces force; specifically, the normal component of the flux density contributes to tangential force (torque), while the tangential component causes normal forces between the stator and rotor [4]. As a result, the SSSR configuration exhibits lower torque and higher normal forces between the stator and rotor compared to the double-sided structure when both use the same stator, and it also achieves a lower power-to-mass ratio when the same volume of PMs is used. Due to these challenges and performance limitations, coreless AFPM machines on the market are not single-sided.

In conventional AFPM machines with ferromagnetic core stators, torque production can be calculated using the Maxwell stress tensor. In this context, the tangential component of the stress tensor, responsible for torque generation, is directly proportional to the tangential flux density in the air-gap. This relationship was examined in [58], which showed that single- and double-sided conventional AFPM machines with YASA topology exhibit comparable torque capabilities when using the same volume of PMs.

Based on the findings reported in [55], [56], the SSSR topology is a suitable choice for high-speed, low-power applications as the absence of the second rotor eliminates normal forces between rotors compared to a double-sided topology, though requiring a detailed investigation of AC losses. The normal forces between the stator and rotor remain low due

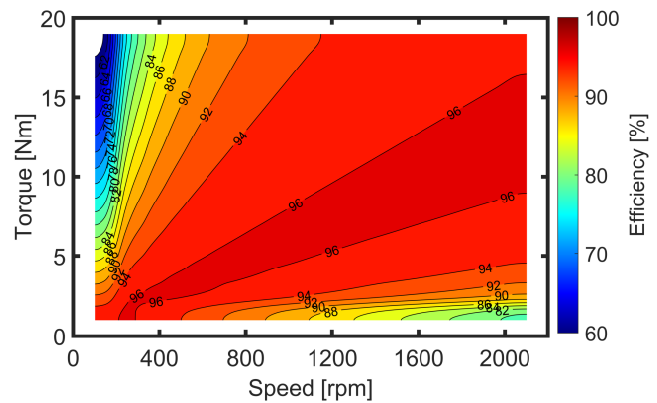


Fig. 10. Efficiency map for an example single-stator double-rotor design rated at 19Nm and 2,100 rpm.

to the machine's reduced power and current loading, resulting in lower mechanical stress. From a cost perspective, using a single rotor reduces the amount of PM material required, and the lower mechanical stress allows for more economical mechanical components and bearings.

The higher tangential flux density also results in higher eddy current losses in the stator conductors and a higher normal force acting between the stator and rotor in SSSR compared to the double-sided topology. The high eddy current losses reduce efficiency and increase the heat generated in the stator conductors. Meanwhile, the large normal force increases noises, vibration, and stress on the bearings, reducing their lifespan and increasing friction losses [59]–[61].

An example of normal force density on the stator for an SSSR topology and the double-sided configuration is compared in Fig. 8, indicating higher normal force in SSSR topology. The tangential flux density is also present in double-sided structures, and its magnitude varies with the distance from the rotor surface. This variation leads to different normal force values exerted on conductors depending on their proximity to the rotor surfaces. However, when the rotor is perfectly balanced, the normal forces exerted by the two rotors act in opposite directions on the conductors and effectively cancel each other out.

The normal force between the stator and rotor in an SSSR topology is generally lower than that of a similarly sized conventional cored AFPM machine. This reduction is primarily attributed to the significantly smaller flux density generated by the armature winding in coreless stator designs. As a result, normal force is typically not a critical concern in coreless stator AFPM machines, except in cases where the machines have a very large outer diameter, such as wind turbine generators, or operate at a high current density, such as those designed for electric aircraft propulsion systems. It should also be noted that careful rotor balancing and implementing advanced control algorithms to minimize current harmonics are essential to reducing normal forces and vibrations.

One advantage of using the SSSR topology is improved thermal management. With the stator not confined between two rotors, there is more surface area available for heat sinks

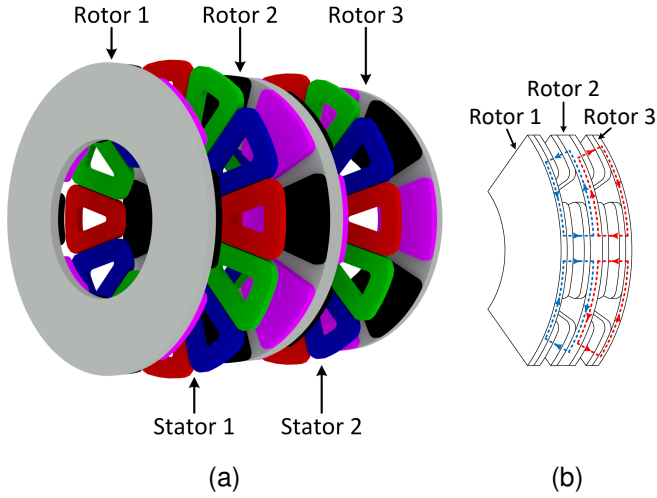


Fig. 11. An example of a multi-stator multi-rotor (MSMR) design featuring a middle rotor with PMs mounted on both sides of the back iron: (a) exploded view and (b) flux pattern within a two-pole-pitch sector of the machine.

or other cooling systems, allowing for more effective heat extraction from the stator. Additionally, there are no inherent limitations on the thermal management system except those imposed by the mechanical size constraints. This flexibility permits the use of larger cooling systems with higher cooling capabilities, enabling the machine to handle higher current densities.

B. Single-Stator and Double-Rotor

A single-stator and double-rotor (SSDR) coreless stator AFPM machine consists of two rotors on either side of a single stator, as shown in Fig. 9. This double-sided structure modifies the air-gap flux path so that flux lines pass axially from one rotor to the other, significantly reducing the tangential component of the air-gap flux density. This configuration balances the normal forces between the stator and rotors, although normal forces between the rotors themselves still occur. To address this challenge, multiphysics design procedures that consider the electromagnetic and mechanical performances of the SSDR topology have been presented in several studies [62]–[65]. Additionally, the AC losses are reduced by an order of magnitude, allowing for the use of thicker conductors and reducing DC losses, which further improves efficiency.

The SSDR topology offers a higher active power-to-mass ratio (specific power density) compared to the single-sided structure. This means that, given the same stator temperature, current density, and PM mass, the SSDR topology generates more power. Due to these advantages, the SSDR topology is the most commonly referenced in coreless stator AFPM machine literature. According to Habib *et al.* [7], more than 65% of the coreless stator AFPM machines discussed in the literature utilize the SSDR topology. This configuration is well-suited for medium-power, cost-effective electric machines used in applications such as fans [17], alternators [19], and electric mobility [22].

The efficiency map of an SSDR coreless AFPM machine, designed for HVAC systems and rated at 19 Nm and 2,100

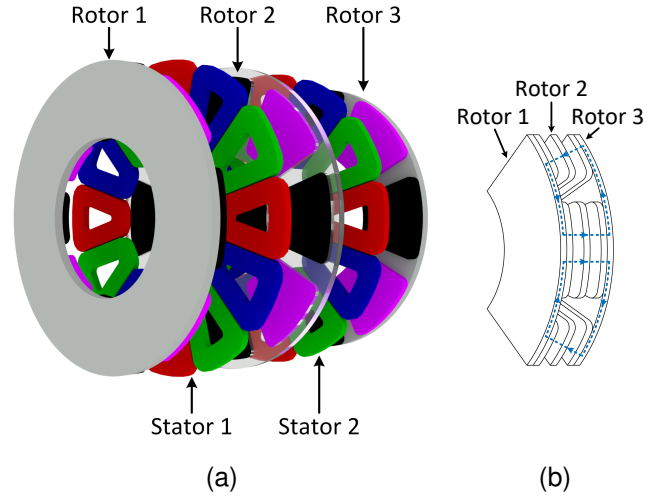


Fig. 12. An example of an MSMR design featuring a middle rotor with PMs embedded in a non-ferromagnetic composite material: (a) exploded view and (b) flux pattern within a two-pole-pitch sector of the machine.

rpm [18], is presented in Fig. 10. Efficiency maps for the conventional cored and coreless machines vary such that the efficiency contours are circular in conventional machines and more linear in coreless ones. Comparing the SSSR and the SSDR of the same rating, the pattern in efficiency contours is the same, however, the overall efficiency is lower. This reduction is attributed to the need for a higher current density to compensate for the lower flux density—resulting from the absence of one rotor—and the increased eddy current losses in the conductors due to the higher tangential flux density component compared to the double-sided topology.

C. Multi-Stator and Multi-Rotor

Enlarging the motor diameter to increase torque in AFPM machines is limited because it increases axial forces on the bearings and adds stress to the mechanical joints between discs and shafts [4]. To meet the required torque without enlarging the machine's diameter, another strategy is to use multiple stacks of AFPM machines. The multi-stators and multi-rotors (MSMR) topology increase output power by maintaining a constant diameter while extending the axial length.

Conventional AFPM machines with iron cores on both the stators and rotors can have various MSMR topology variants based on rotor types and whether the topology features an outer rotor or outer stator. These variants are discussed in [66], [67]. However, such variations are not found in coreless stator AFPM machines due to low specific power density, efficiency, and high normal forces between stators and rotors in outer stator topologies. Therefore, multi-stage coreless stator AFPM machines are typically configured with inner stators consisting of N stators sandwiched between $N + 1$ rotors.

The multi-disk topology within coreless stator AFPM machines has two variants based on the flux pattern and structure of the middle rotor, with examples depicted in Figs. 11 and 12. In the first configuration, termed MSMR-Parallel in this paper, the middle rotor features a yoke with PMs mounted on both sides, forming two parallel magnetic flux paths under

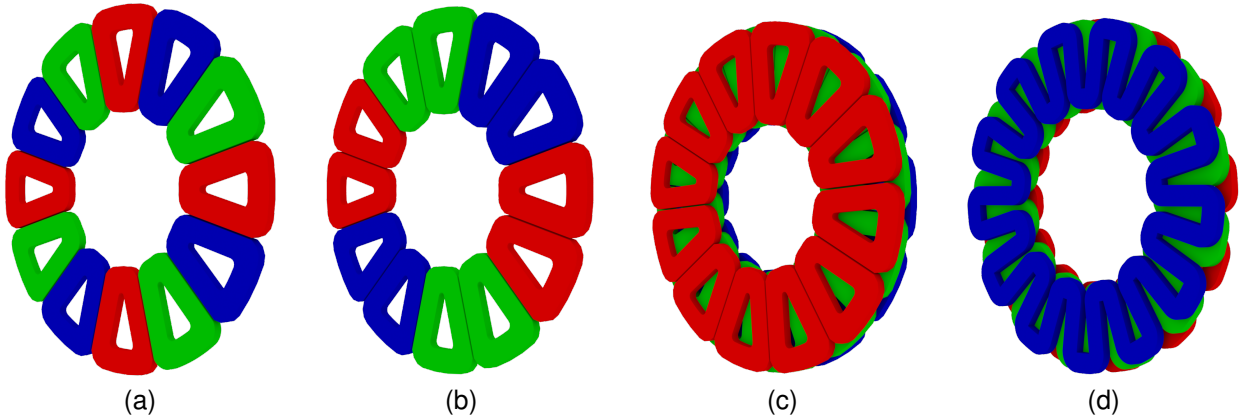


Fig. 13. Example three-phase winding structures employed in coreless stator AFPM machines, including (a) a conventional concentrated winding that may operate with 8 or 16 poles, (b) a phased-group winding that may operate with 10 or 14 poles, (c) an overlapping (distributed) winding that may operate with 12 poles, and (d) a wave winding that may operate with 26 poles.

each pole, as illustrated in Fig. 11a. The magnetic flux lines for this topology are displayed in Fig. 11b, indicating that the flux lines are enclosed through the middle rotor yoke, one air-gap, and an outer rotor back iron.

While the outer rotors are the same as in the MSMR-Parallel, the middle rotor of the MSMR-Series uses a single layer of magnets embedded in a composite non-ferromagnetic material with the structure of this topology is illustrated in Fig. 12a. The flux lines under each pole in the MSMR-Series have longer paths compared with the MSMR-Parallel, as they pass through two rotor back irons and multiple air-gaps, as shown in Fig. 12b. If the back-to-back PMs in the middle rotor of an MSMR-Parallel have the same magnetization direction, the machine can be classified as MSMR-Series.

The first coreless AFPM machine with MSMR topology was proposed, designed, and prototyped by Eastham *et al.* [5], [24], [45] for use in stratospheric aircraft propeller drives. They utilized plastic materials as the support structure for the middle rotors and stators, rather than aluminum, to mitigate eddy current losses and improve overall specific power density.

Taran *et al.* [23] concluded that MSMR coreless AFPM machines can achieve higher specific power density and greater efficiencies compared to single-disk conventional cored AFPM machines, although the coreless type exhibits more torque limitations when using the same thermal management system. Vatani *et al.* [33] showed that the MSMR coreless AFPM machine not only provides higher specific power density compared to its SSDR counterpart but also enhances reliability through redundancy techniques. They also discussed that the surface area available for heat extraction increases proportionally with the number of stacks, allowing for better thermal management.

In an ideal scenario, the axial forces between the rotors within an MSMR topology are balanced due to equal air-gaps on both sides. However, manufacturing imperfections can lead to significant axial forces between the rotors, especially in applications with larger outer diameters, such as direct-drive wind turbine generators. Mueller *et al.* [20], [28], [68], [69] designed and prototyped MSMR coreless stator AFPM generators for direct wind turbine and tidal current turbine

applications. To control the axial forces between rotors and reduce stress on the bearings, they proposed a C-shaped mechanical structure for the rotor. This structure transfers the axial forces to the C-shaped frame instead of the bearings, thereby improving the overall reliability and performance of the generator.

Coreless AFPM machines with MSMR topology have been proposed for multiple applications, ranging from electric aircraft and electric vehicles to direct-drive wind turbine generators. Examples of literature employing MSMR topology can be found in the following sources: [70]–[89].

IV. WINDING

Windings in coreless AFPM machines can have a variety of configurations and be implemented with different materials. This section reviews the types of windings, materials, and manufacturing techniques used in coreless stator AFPM machines, as found in the literature.

Although various winding topologies and configurations exist in the literature, windings in coreless stator AFPM machines can generally be categorized into three types: overlapping, non-overlapping (or concentrated), and phase group non-overlapping windings [4]. Figure 13 illustrates the topology and coil arrangement for each of these winding types in a three-phase coreless stator AFPM machine.

In overlapping windings, depicted in Figs. 13c and 13d, the coils of different phases overlap each other. Conversely, non-overlapping windings, shown in Fig. 13a, consist of coils that do not overlap, with all coils positioned in a single layer. Lastly, phase-group windings, as shown in Fig. 13b, are a variant of the non-overlapping type, featuring a distinct coil arrangement compared to conventional non-overlapping.

A. Overlapping Windings

Among the winding types in coreless stator AFPM machines, overlapping (distributed) windings offer the highest output torque due to their superior winding factor compared to non-overlapping types [90], [91]. However, this advantage comes with specific challenges, including increased complexity in coil assembly and manufacturing, as well as a longer

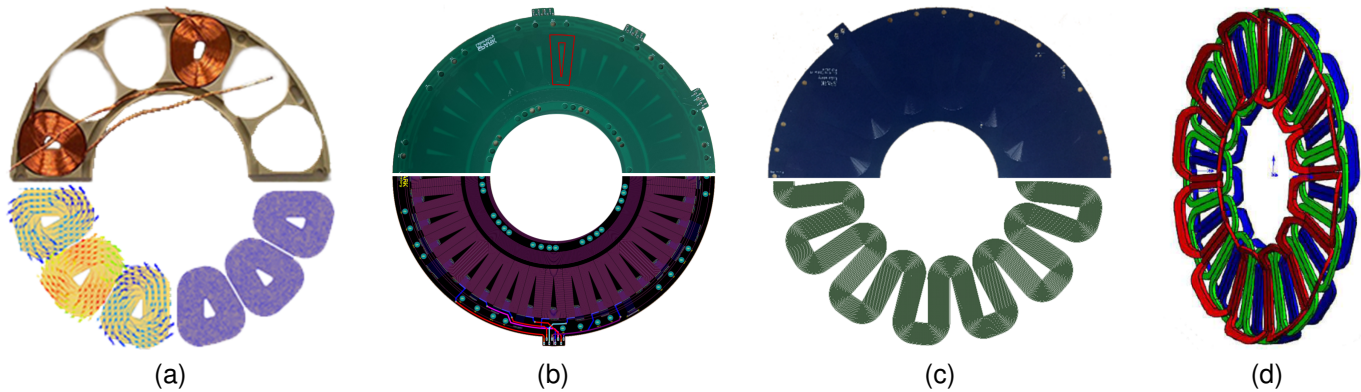


Fig. 14. Example coreless machines with varying winding types including (a) a coreless stator with a concentrated winding structure prototyped by Eastham *et al.* [5], a PCB stator with (b) concentrated and (c) wave winding structures designed by the SPARK research group [18], [92], and (d) a bent end-winding concept with overlapping winding to place all active coil segments at the same distance from the rotor [93].

end-winding length compared with non-overlapping windings. The longer end winding leads to higher copper losses without enhancing output torque, thereby reducing overall machine efficiency. Figures 13c and 13d illustrate common structures of overlapping windings, showing the regular and wave overlapping configurations, respectively.

The overlapping winding shown in Fig. 13c is a three-layer winding, each corresponding to a single phase. Within each phase, the number of coils matches the number of poles, with two adjacent coils positioned under two opposite poles. As a result, these adjacent coils are wound in opposite directions. Finally, the coils are connected in series to meet the induced voltage and to form the phase. The overlapping wave winding shown in Fig. 13d features a similar three-layer structure, where the number of poles equals the number of coil sides.

Jore *et al.* [47] introduced a new manufacturing method for overlapping windings using a PCB stator, which significantly reduces the complexity of the manufacturing process. Their approach involves using separate PCBs for different parts of the winding, including the coil sides and inner and outer end windings. After positioning the coil sides in their appropriate locations, the end windings are connected through designated holes and axial bars. While this method simplifies the manufacturing of overlapping windings, it may not be ideal for machines with a high number of poles and coils due to the increased number of necessary connections. Additionally, this method results in a relatively large end-winding length, which contributes to increased copper and eddy current losses.

In coreless stator AFPM machines, the normal component of the air-gap flux density directly contributes to torque production, and its value decreases exponentially with increasing distance from the magnet surface. In conventional overlapping windings, each phase is positioned in a single layer at varying distances from the rotor surface. This arrangement causes the phase located farther from the rotor surface in SSSR topology and the phase sandwiched between two others in SSDR topology to experience lower flux density, leading to unbalanced back EMF and potentially increased torque ripple.

To address this issue, Smith *et al.* [94] introduced a six-layer winding configuration instead of the standard three layers and

employed a transposition technique to achieve balanced back EMF. Another approach to balancing the back EMF involves shaping the end winding so that the coil sides of different phases are equidistant from the rotor surface [93], [95], [96], as illustrated in Fig. 14d. However, this method restricts the coil side width, which is directly related to the torque capability in coreless AFPM machines.

Wave winding construction helps reduce the end-winding length in overlapping windings [92], [97] but does not resolve the issue of differing induced voltage levels between layers. To address this, Greaves *et al.* [98] proposed a new manufacturing technique for wave windings. They implemented a winding configuration similar to a two-layer wave winding used in conventional cored machines. This approach results in a two-layer winding where the induced voltage in all phases is balanced while benefiting from the reduced end-winding length of wave windings. This implementation offers the potential for a very high winding factor and enhanced torque production capability. Further examples of wave winding applications in coreless AFPM machines can be found in [99]–[101].

B. Concentrated Windings

Most existing coreless stator AFPM machines utilize regular non-overlapping windings, also known as concentrated windings. The concentrated winding adopts a similar structure to that of conventional cored machines. The example concentrated winding illustrated in Fig. 13a consists of twelve coils and can operate with 8 or 16 poles. In this design, consecutive coils are wound in the same directions and connected in series to form a phase.

Although concentrated windings typically exhibit a lower winding factor and torque capability than overlapping windings, their performance can be comparable or even superior in specific pole-to-coil ratios, such as 4/3 and 14/12 [102] for coreless AFPM machines. Additionally, the manufacturing process for concentrated windings is significantly more straightforward compared to overlapping windings, particularly in fully automated winding constructions with PCBs.

Eastham *et al.* [24] calculated and compared the total winding factor for three different winding configurations: a

three-layer overlapping winding, a concentrated winding with a 120-degree electric coil span, and a concentrated winding with a 240-degree electric coil span. Their calculations showed that the concentrated winding with a 240-degree electric coil span had the highest winding factor, even surpassing that of the distributed winding. Xia *et al.* [103] compared three types of windings: regular and wave-type three-layer overlapping windings and a two-layer concentrated winding with a 240-degree electric coil span. In the concentrated winding, the two layers are similar but have a 180-degree electric phase shift. Their results indicated that the concentrated winding produced more torque than its overlapping winding counterparts.

Concentrated windings produce more MMF harmonics compared to overlapping windings. While this may not pose a significant issue in coreless AFPM machines due to their low armature reaction, it can lead to considerable losses in the rotor back iron and magnets if they operate under high electric loading or speeds. To address this, Rallabandi *et al.* [104], [105] proposed a multi-layer concentrated winding to reduce non-torque-producing MMF harmonics in coreless stator AFPM machines. Their approach involved dividing the concentrated winding into multiple layers and appropriately shifting them, which allowed the stator MMF to become comparable to that of overlapping windings and reduced rotor losses due to MMF harmonics to 5% of those in the single-layer winding configuration.

The geometric shape of the concentrated coils also affects torque production and harmonic distribution. For example, the circular-shaped concentrated winding studied in [73], [106]–[108] offers advantages in manufacturing simplicity and low harmonic values but has significantly lower torque capability compared to trapezoidal coil windings. On the other hand, a hexagonal-shaped concentrated coil, as studied in [109], [110], aims to reduce copper loss, albeit at the expense of reduced output torque compared to trapezoidal coil windings.

C. Phased-Group Winding

In phase group windings, such as the example shown in Fig. 13b, the stator's periphery is divided into sections corresponding to the number of phases, with the coils of each phase positioned adjacent to one another. This arrangement simplifies the electrical connections between coils of the same phase due to their proximity. Additionally, phase group windings tend to have lower harmonic values compared to concentrated windings [91].

Multiple phase group windings for coreless AFPM machines have been explored in the literature concerning weight optimization and slot-pole combinations [111]–[114]. Phase-group winding can be designed with pole-to-coil ratios of 10/12 or 14/12, grouping two consecutive coils per phase, or 8/9 or 10/9, grouping three consecutive coils per phase. For other pole-to-coil ratios, the winding factor can be significantly lower, which limits torque production.

D. Advanced Winding Materials

A significant portion of the literature on coreless stator AFPM machines focuses on material investigations for the



Fig. 15. Exploded view of an example coreless AFPM machine with a multi-layer PCB stator produced by Core Motion Inc. [119].

stator, particularly the use of printed circuit board (PCB) stators. This type of stator offers repeatable, low-cost, and highly reliable production capabilities, making them well-suited for rapid mass production [9], [89]. Their computer-aided design and automated manufacturing processes eliminate the complexities associated with winding production using regular or Litz wires [115], [116]. A comprehensive review of PCB stator windings for coreless or slot less AFPM machines is presented in [117]. Kesgin *et al.* [118] also explored the design aspects of Litz wire and PCB stators in coreless AFPM machines, offering a brief overview of the state-of-the-art PCB winding technology.

Figures 14b and 14c showcase PCB stators employing regular and wave overlapping windings, designed by the SPARK research group. Compared to traditional designs, as shown in Fig. 14a, the use of PCB technology can result in significant cost and time savings, especially in mass production scenarios. However, one major drawback of PCB stators compared to Litz wire is their lower copper fill factor with current PCB technologies [115], which limits their application in high-performance motors [21]. The design considerations, optimization, and mathematical modeling of coreless AFPM machines with PCB stators have been extensively discussed in the literature, including references such as [120]–[122].

Another design challenge for PCB stators is mitigating eddy current losses in the conductors. While Litz wire reduces conductor eddy current loss through multiple strands and transposition, similar techniques must be manually integrated into the design of PCB stators [18]. This requires a coil configuration capable of accommodating full conductor transposition in multi-layer PCB technology, which limits the selection of pole numbers and the pole-to-coil ratio. To fully leverage the advantages of PCB stators, a multiphysics design approach is necessary to balance loss mitigation and thermal performance. Several studies have employed multiphysics design for PCB stators in coreless AFPM machines to analyze their thermal and loss behavior [123]–[126].

The industry showed a keen interest in coreless AFPM machines with PCB stators, leading to the emergence of several companies, such as Infinitum, that produce these machines in various sizes for the market. Another notable example is Core Innovation, which was licensed in 2009 to develop a

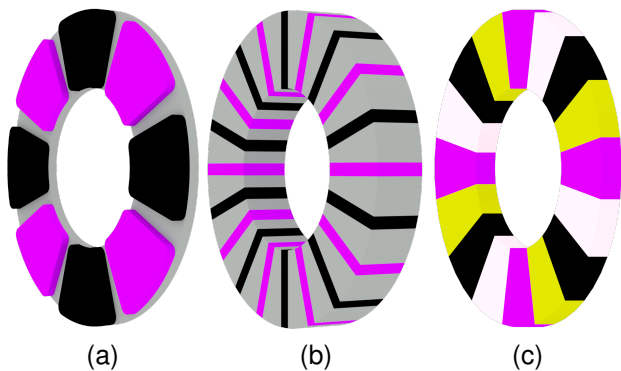


Fig. 16. Example rotor types that can be employed for coreless stator or fully coreless AFPM machines, including (a) a surface-mounted PM rotor, (b) a spoke-type PM rotor, and (c) a Halbach array rotor.

PCB stator AFPM generator based on a previously presented concept, shown in Fig. 15, for a direct-drive wind turbine project sponsored by the U.S. Department of Energy [119].

Another promising stator material for coreless AFPM machines is carbon nanotube (CNT) wires. Recent advancements in CNT technology have opened up significant potential for their use in electromagnetic devices. CNT wires offer several advantages, including low mass density, negligible skin effect, and a low coefficient of resistance increase with temperature. Rallabandi *et al.* [79], [127] explored the feasibility of using CNT windings in coreless stator AFPM machines and provided a systematic design procedure. Their study suggested that the power-to-mass ratio of coreless AFPM machines with CNT stators is higher than that of machines using copper. For the same power output, the weight of machines with CNT coils is only 66% of that of machines with copper coils.

E. Mutual Coupling and Mitigation Techniques

The ratio of mutual to self-inductance in the windings of a coreless machine is comparable to that of a conventional machine at approximately one-third [9]. This ratio can vary depending on the winding type and configuration, yet a comprehensive review of this topic is lacking in the literature. While the low mutual inductance may not initially appear critical, the higher short-circuit fault current in coreless machines than in conventional machines can pose a challenge, potentially disrupting the regular operation of other phases.

For electric aircraft propulsion, mutual coupling between phases is a critical factor as it directly affects the machine's fault-tolerant capability. Coreless AFPM machines offer inherent geometric advantages that help reduce or mitigate the effects of phase coupling. One approach is to use a two-phase winding as the phases are electrically perpendicular such that mutual coupling between phases is eliminated [128]. This method is particularly suitable for overlapping windings like the examples depicted in Figs. 13c and 13d.

To convert from the three-phase winding to a two-phase configuration, one phase can be removed, and the angular difference between the remaining two phases can be adjusted from 120 to 90 electrical degrees. As shown in [9], eliminating one phase in coreless AFPM machines with overlapping

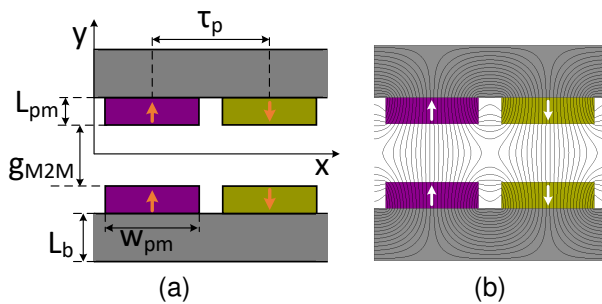


Fig. 17. An unrolled 2D view of two pole pitches of an example surface-mounted PM rotor showing (a) geometrical parameters used for the analytical flux density calculation and (b) magnetic flux line distribution.

winding structures results in a smaller M2M gap, which leads to higher flux density and compensates for the reduction in the number of phases. Therefore, a two-phase overlapping winding coreless AFPM machine can potentially perform as effectively as a three-phase machine, with the added benefit of eliminating mutual coupling between phases.

Another approach, discussed in [129], involves using two identical stators of any type, which are separated by a ferromagnetic disk. This disk is connected to the shaft and rotates at synchronous speed along with the PM rotors. The ferromagnetic plate effectively short-circuits the magnetic flux produced by each stator, mitigating the coupling between stators with the trade-off of slightly increased mass and volume.

V. ROTOR

Coreless AFPM machines can be designed using one of three rotor types, as illustrated in Fig. 16: surface-mounted PM, spoke-type PM, and Halbach array PM. This section describes and compares these rotor types, with a particular emphasis on the Halbach array, which is particularly appealing for electric motors proposed for electric aircraft propulsion. Additionally, the flux density distribution equations for the two most prevalent rotor topologies, surface-mounted PM and Halbach array, are presented.

A. Surface-mount

The surface-mounted PM rotor consists of multiple PMs mounted on a back iron, with alternating polarities positioned adjacent to each other. This rotor type is the most commonly used in coreless stator AFPM machines due to its straightforward manufacturing process and potentially lower cost compared to the other rotor variants, as it requires less PM materials for a given outer diameter. The essential geometric parameters for this rotor type include the ratio of pole arc to pole pitch, PM length, back iron thickness, and pole number.

The impact of these geometrical parameters on the performance of a coreless AFPM machine with a surface PM rotor can be captured from this rotor type's flux density equation. Considering a cylindrical cut at an arbitrary radius for two pole pitches of an example axial flux double-sided surface-mounted PM rotor and unfolding it results in a 2D linear design as shown in Fig. 17a and with its flux line distributions shown in

Fig. 17b. For this 2D model, the normal and tangential air-gap flux density components can be calculated from [130]:

$$B_x = 4B_r \sum_{i=0}^{\infty} B_{n_{SPM}} \sinh\left(\frac{n\pi y}{\tau_p}\right) \sin\left(\frac{n\pi(2x + \tau_p)}{2\tau_p}\right) \quad (1)$$

$$B_y = 4B_r \sum_{i=0}^{\infty} B_{n_{SPM}} \cosh\left(\frac{n\pi y}{\tau_p}\right) \cos\left(\frac{n\pi(2x - \tau_p)}{2\tau_p}\right), \quad (2)$$

where B_r is the remanence of the PMs, $n = 1 + 2i$ with i denoting the harmonic order, τ_p represents the pole pitch, and x and y are positions in the Cartesian coordinates. The value of B_n can be derived from:

$$B_{n_{SPM}} = \frac{\sin(n\pi w_{pm}/2\tau_p)}{n\pi} \frac{\sinh(n\pi L_{pm}/\tau_p)}{\sinh(n\pi(L_{PM} + g_{M2M}/2)/\tau_p)}, \quad (3)$$

where w_{pm} denotes the width of the PM, L_{pm} represents the length of the PM, and g_{M2M} is the magnet-to-magnet gap distance. It should be noted that these equations were derived under the assumption of infinite relative permeability for the back iron, and therefore, do not account for saturation.

The effect of the PM axial length is modeled using a hyperbolic sinusoid, which indicates that a longer PM length results in increased air-gap flux density. However, it is essential to consider the ratio of PM length to pole pitch, as seen in (3); a larger pole pitch necessitates a proportionally longer PM length. For the magnet-to-magnet gap g_{M2M} , the relationship is modeled using an inverse hyperbolic sinusoid, suggesting that the flux density decreases exponentially as g_{M2M} increases. This parameter is also influenced by the pole pitch, as a larger pole pitch allows for a greater g_{M2M} . With a larger g_{M2M} , there is more space to accommodate additional conductors in the air-gap of a coreless AFPM machine, potentially increasing the torque produced.

The pole pitch, which depends on the number of poles, is a crucial design parameter for this rotor type as it influences all other geometrical variables. Therefore, during the design optimization process, the pole number should be treated as an independent variable, with other geometrical parameters—including w_{pm} , L_{pm} , and g_{M2M} —normalized based on the pole pitch. It is evident that a lower pole number enables larger w_{pm} and L_{pm} , which increases the magnetic loading and allows for a wider g_{M2M} to accommodate more conductors. However, this comes at the cost of increased mass.

The ratio of PM width to pole pitch is an influential geometric parameter in a coreless AFPM machine. Although increasing this ratio might initially suggest higher flux density and torque production, it also leads to greater flux leakage between adjacent poles, limiting the torque enhancement. This ratio has no specific optimal value, as it is highly dependent on other geometrical variables, such as the magnet-to-magnet gap, pole number, and outer diameter, requiring a trade-off between these parameters. The literature suggests that a ratio of approximately 0.8 is generally preferable, as indicated in [18], [131]. This ratio also influences the required thickness of the back iron; a larger pole arc to pole pitch ratio necessitates

a thicker rotor back iron to prevent core saturation.

In coreless AFPM machines, the back iron is typically made from solid ferromagnetic material, offering a significant advantage over cored machines due to the reduced armature reaction. However, when operating under heavy electric loading, as is common in electric aircraft applications, the stator MMF harmonics can induce eddy current losses, requiring the use of laminated steel. Fabricating laminated steel for AFPM machines is more challenging than for radial flux machines because the electrical steel layers must be stacked radially. The methods for fabricating laminated cores in AFPM machines were reviewed in [4].

In surface-mounted PM rotors, the magnets are typically trapezoidal, featuring a single arc angle and varying widths across different radii. The shape and arrangement of the PMs significantly influence the harmonic distribution and magnitude of the air-gap flux density. Taqavi *et al.* [132] compared various PM geometries, including trapezoidal and circular-shaped magnets. Circular-shaped magnets are thin cylindrical magnets magnetized in the axial direction. Their study concluded that trapezoidal-shaped magnets achieve the highest air-gap flux density, whereas circular-shaped magnets generate a more sinusoidal flux waveform. Circular-shaped magnets are more cost-effective compared to trapezoidal PMs and have been investigated in several studies, including those reported in [73], [107], [108], [133].

In another study, Praglowska [134] reported that horseshoe-shaped PMs achieve the highest air-gap flux density and are the most effective, although the trapezoidal shape was not considered in this study. Additionally, Yazdi *et al.* [135] proposed a novel topology for surface-mounted rotors, which combines features of surface-mounted PMs and spoke-type rotors. This design enhances the air-gap flux density at a constant pole number by incorporating tangentially magnetized PMs in the back iron.

B. Spoke-type

The spoke PM rotor, also known as a flux-focusing rotor, consists of PMs magnetized tangentially to the air-gap and positioned between ferromagnetic cores. A 3D view of an example axial flux spoke rotor is shown in Fig. 16b. This rotor type has been widely studied in the literature for both radial and axial flux machines with cored structures, primarily due to its significant advantage of high flux concentration. This results in more efficient use of PM material [136] and offers the potential for designs with very few stator coils using high rotor pole counts, thereby simplifying stator winding manufacturing [137].

Multiple researchers have studied the use of spoke rotors within coreless stator structures for two primary reasons: (1) the spoke-type rotor in cored machine structures suffers from relatively high torque ripple and cogging torque, which can be mitigated by employing a coreless stator, and (2) to leverage the flux concentration capability of this rotor type in coreless stator configurations. Marcolini *et al.* [138] discussed and compared the design considerations of a coreless AFPM with surface-mounted PM and spoke rotors using equivalent 2D

FEA. Their study indicated that the spoke rotor allows for a larger magnet-to-magnet gap, enabling the accommodation of more conductors.

The spoke-type rotor cannot be used within an SSSR coreless AFPM machine, as an opposing rotor is required to attract the flux lines and guide them through the air gap. Without this opposing rotor, half of the PM flux travels in the opposite direction, failing to contribute to torque production.

In an SSSR coreless AFPM machine with spoke rotors, flux leakage occurs on the rotor side that does not face the air gap. This leakage results from the large gap between rotors in coreless stator machines and does not contribute to torque production. This flux leakage can be mitigated to some extent by optimizing the shape of the PMs. For example, Marcolini *et al.* showed that a rotor flux leakage and higher air-gap flux density could be achieved when the PMs are rectangular shape and the core segments are trapezoidal shape [138].

Other variations of spoke-type rotors have been explored to enhance air-gap flux density further. Aydin *et al.* [139] investigated a coreless stator with sinusoidal-shaped rotor core segments, demonstrating a significant improvement in air-gap flux density compared to conventional spoke rotors. However, this sinusoidal pole shape introduces additional manufacturing complexity. Radulescu *et al.* [140] proposed a modification to the spoke rotor by incorporating a normally magnetized PM within the rotor core segments, creating a quasi-Halbach configuration. This design not only increases air-gap flux density due to the added PM but also improves flux line guidance towards the air-gap, thereby reducing flux leakage on the opposite side. Nevertheless, this approach also complicates the manufacturing process.

The flux concentration capability of spoke rotors enables the use of cost-effective magnets, such as ferrite, in large-scale and cost-sensitive designs. Chirca *et al.* [141]–[144] leveraged this advantage to propose a coreless stator AFPM machine with a double-sided spoke rotor for micro-wind power applications. By optimizing the spoke rotor’s geometry to maximize flux concentration, they achieved a maximum air-gap flux density of 0.52 T despite the ferrite magnets’ remanence being 0.4 T.

C. Halbach Array

This subsection presents a thorough literature review on the Halbach array rotor, examining it from geometrical, performance, application, and field analysis perspectives. Given the high interest in Halbach PM array rotors for electric machines in aircraft propulsion systems, this review is more comprehensive than the two previous subsections. Additionally, while the primary focus of this paper is on coreless AFPM machines, this subsection also covers the application of the Halbach array in conventional cored machines.

The concept of the Halbach array was first introduced by John C. Mallinson in a 1973 paper [145]. Mallinson demonstrated a previously unrecognized class of magnetization patterns in planar structures with the unique property that all magnetic flux emerges from one surface while none exits the opposite side, as exemplified by a constant-amplitude rotating vector magnetization where the rotation direction dictates

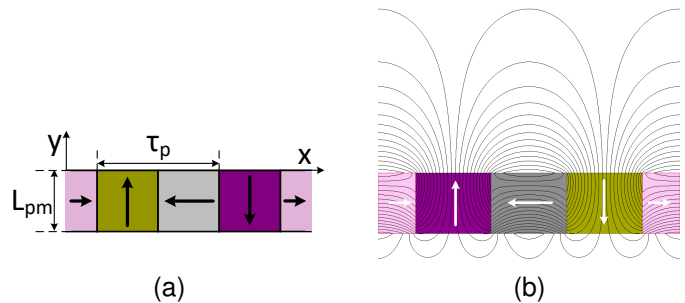


Fig. 18. An unrolled 2D view of a single rotor in a typical Halbach PM array: (a) geometrical variables and coordinate definitions; and (b) magnetic flux line distribution showing the concentration of flux on one side while minimizing it on the other side.

the flux-free surface. The practical implementation of this concept using PM was later demonstrated by Klaus Halbach [146], who aimed to achieve strong, sinusoidal magnetic fields with rare-earth cobalt PMs. Halbach further developed the analytical equations governing the magnetic field in such PM arrangements in [147]. The Halbach PM array is named in recognition of his contributions to the theory and development of one-sided flux PM configurations.

The Halbach PM array rotor consists of discrete PM segments, each with a magnetization vector oriented at different angles relative to the axial direction. The simplest form of a Halbach array, illustrated in Fig. 18, comprises four magnets per wavelength: two are axially magnetized toward the air gap, while the other two are tangentially magnetized.

The Halbach PM array weakens the magnetic flux on one side while intensifying it on the other, as shown in Fig. 18b. The flux lines complete their path through the tangentially magnetized PMs, allowing for the elimination of the rotor back iron, which reduces the rotor mass. This improvement in rotor mass directly enhances the specific power density of electric motors, making Halbach PM array rotors highly attractive for electric aircraft applications.

To compare the performance of a Halbach PM array rotor with a conventional surface-mounted PM rotor, consider a double-sided linear surface-mounted PM rotor where the magnet span equals the pole pitch, meaning the entire rotor surface is covered with magnets of uniform size but alternating polarity. Now, assume a double-sided Halbach array rotor with magnets of the same length as those in the surface PM rotor and without a back iron. In this scenario, both rotors use the same amount of magnet material, but the Halbach variant lacks rotor back iron. Under these conditions, the surface PM rotor exhibits a higher air-gap flux density. Therefore, while the Halbach array rotor is lighter due to rotor back iron elimination, it still requires more magnet material to achieve comparable performance to the surface PM rotor.

In a study conducted by Chulaee *et al.* [148], it was concluded that in the scenario described earlier, if the PM length in the Halbach array is increased to match the total length of the surface PM rotor—including both the PM and back iron—the Halbach configuration achieves approximately 30% higher flux density. Assuming the same mass density

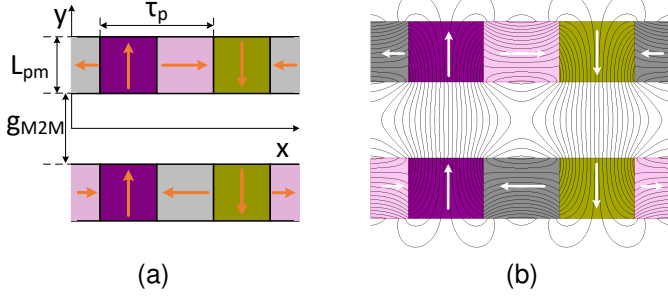


Fig. 19. An unrolled 2D view of two rotors each using an example Halbach PM array with (a) geometrical parameters used for the analytical flux density calculation and (b) flux line distribution.

for both the PM material and electric steel, this translates to a 30% increase in specific torque density for the Halbach array within the same rotor mass and overall dimensions. To achieve the same performance as a surface-mounted PM rotor, a Halbach rotor would require less overall mass, making it a more lightweight alternative.

These observations suggest that the Halbach array is advantageous in applications where minimizing mass is a higher priority than cost. However, to achieve the required torque with minimal mass in a machine utilizing a Halbach PM array rotor, careful consideration must be given to the geometrical parameters of the array. The following paragraphs review the equations governing the air-gap flux density of the Halbach array and discuss the impact of these variables.

First, the normal component of air-gap flux density for a linearized single-sided Halbach PM array rotor is presented. This formulation is applicable for field analysis in conventional machines with small air-gaps and cored structures, as well as in single-stator and single-rotor (SSSR) coreless AFPM machines. The air-gap flux density of a single-sided Halbach PM array can be calculated from [149]:

$$B_y = B_r \sum_{i=0}^{\infty} \frac{\sin(\epsilon n \pi / m)}{n \pi / m} \left[1 - \exp\left(\frac{-n \pi L_{pm}}{\tau_p}\right) \right] \exp\left(\frac{-n \pi y}{\tau_p}\right) \sin\left(\frac{n \pi x}{\tau_p}\right), \quad (4)$$

where ϵ is typically set to one, $n = 1 + mi$, with m representing the number of PMs per wavelength and i denoting the harmonic order. B_r is the remanence of the PMs, L_{pm} is the PM length, $\tau_p = \frac{\pi D}{P}$ is the pole pitch, where D is the arbitrary diameter and P is the number of poles. The variables x and y refer to the positions along the x and y axes, as defined in Fig. 18a.

The flux density distributions between two Halbach array disks, shown in Fig. 19a, are calculated in [147], [150] by solving Poisson equations and using Fourier transform as:

$$B_x = B_{n_{Hal}} \sinh\left(\frac{n \pi y}{\tau_p}\right) \cos\left(\frac{n \pi x}{\tau_p}\right), \quad (5)$$

$$B_y = B_{n_{Hal}} \cosh\left(\frac{n \pi y}{\tau_p}\right) \sin\left(\frac{n \pi x}{\tau_p}\right), \quad (6)$$

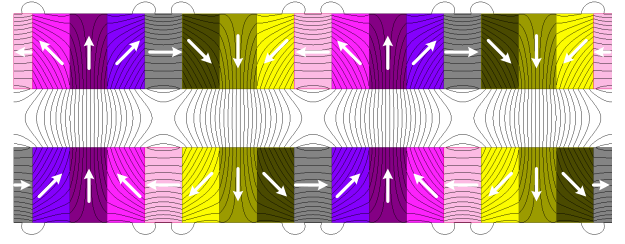


Fig. 20. An unrolled 2D view of flux line distribution for an example Halbach PM array with eight PMs per wavelength (four in pole pitch).

where $B_{n_{Hal}}$ can be calculated from:

$$B_{n_{Hal}} = 2B_r \sum_{i=0}^{\infty} \frac{\sin(\epsilon n \pi / m)}{n \pi / m} \left[1 - \exp\left(\frac{-n \pi L_{pm}}{\tau_p}\right) \right] \exp\left(\frac{-n \pi g_{M2M}}{2 \tau_p}\right) \quad (7)$$

where g_{M2M} is the magnet-to-magnet gap distance.

The flux density equations for the Halbach PM array show that the number of PMs per wavelength significantly influences the flux density amplitude and its harmonic spectrum. Robertson [151] and Ubani *et al.* [152] both observed that the flux density amplitude increases with a higher number of PMs per wavelength. This trend can also be deduced from the term $\frac{\sin(\epsilon n \pi / m)}{n \pi / m}$, where, for the fundamental component ($n = 1$), the value of the term increases as m increases. Figure 20 shows the flux line distribution for a Halbach array with $m = 8$, where the design features the same PM dimensions as the design with $m = 4$ shown in Fig. 19b. The figure illustrates a reduction in flux leakage on the side not facing the air-gap for the design with a higher number of PMs per wavelength.

Vatani *et al.* [130] indicated that increasing m from four to eight enhances the flux density amplitude by approximately 10%; however, increasing it further from eight to twelve does not result in additional flux density amplification. They also analyzed the air-gap flux density's harmonic spectrum, which causes stator eddy current losses and concluded that the harmonic content significantly diminishes when m changes from 4 to 8, with negligible harmonics observed for $m = 12$. Galea [153] investigated the impact of the number of PMs per wavelength on the demagnetization of the Halbach PM array. The study indicated that when $m = 4$, there is negligible demagnetization at the corners of the tangential PMs under no load; however, this can become critical at high operating temperatures. In contrast, when $m = 8$, the risk of demagnetization is significantly reduced.

The next Halbach array geometrical variable to discuss is the PM axial length L_{PM} . Ubani [131] conducted parametric studies based on (7) which indicated that the air-gap flux density increases approximately linearly with increasing L_{PM} until it reaches half the pole pitch. Beyond this point, the flux density continues to increase with further enlargement of L_{PM} , but at a reduced rate, and it ceases to increase for L_{PM} values exceeding one pole pitch. Although a larger L_{PM} enhances flux density, this comes at the cost of increased mass, making it crucial to determine the optimum L_{PM} for the

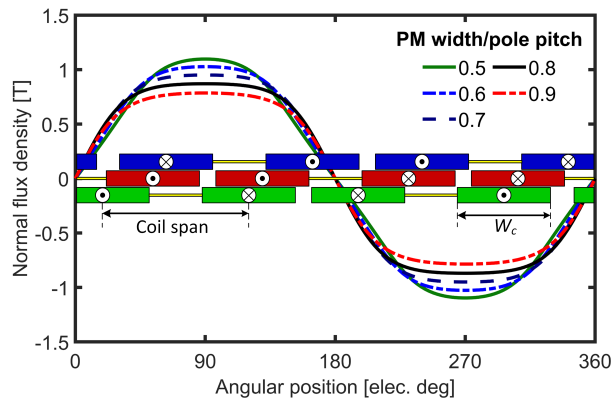


Fig. 21. Air-gap flux density at the midpoint of the air gap for an example design of a double-sided Halbach array, illustrating variations in flux density with differing widths of the normally and tangentially magnetized magnets while maintaining a constant pole pitch.

Halbach PM array rotor to achieve the highest specific power. A parametric study based on the flux density equations for PM length in [130] showed that the optimum L_{PM} in terms of specific power depends on the magnet-to-magnet gap (g_{M2M}). They showed that the optimal range for L_{PM} is between 0.25 and 0.4 times the pole pitch, with larger g_{M2M} requiring a correspondingly larger PM length.

The final geometrical parameter, particularly important for coreless machines, is the g_{M2M} . A larger g_{M2M} allows for more conductors in the air-gap, which increases the torque. However, this comes at the cost of increased machine mass and reduced efficiency. A parametric study similar to the one conducted for L_{PM} was performed to assess the impact of g_{M2M} on specific power density, as reported in [130]. The study found that the optimal g_{M2M} occurs when it is between 0.35 and 0.5 times the pole pitch, depending on L_{PM} . Additionally, since copper losses rise with larger g_{M2M} due to the increased conductor volume in the air-gap, careful consideration must be given to thermal management.

Both L_{PM} and g_{M2M} depend on the pole pitch, which is determined by the number of poles. Consequently, the number of poles influences the machine's magnetic and electric loading. For a given outer diameter, low pole numbers require larger L_{PM} and g_{M2M} to achieve their optimal ranges, as discussed in the previous paragraph. This increases the magnetic and electric loading of the machine, albeit at the expense of higher mass. Therefore, if the L_{PM} and g_{M2M} are to be selected based on their optimal ranges, the key remaining decision is the number of poles.

The discussions on the geometric variables of the Halbach array PMs presented so far assume equal widths for PMs magnetized normally and tangentially. A parametric study in [154] indicated that using a wider PM width for the normally magnetized magnets expands the normal flux density window in the air-gap. This also leads to a decrease in flux density amplitude due to increased flux leakage on the side of the Halbach array that does not face the air-gap, necessitating the use of a back iron as exemplified in [153], [155].

In a coreless AFPM machine with a rotor utilizing a Halbach

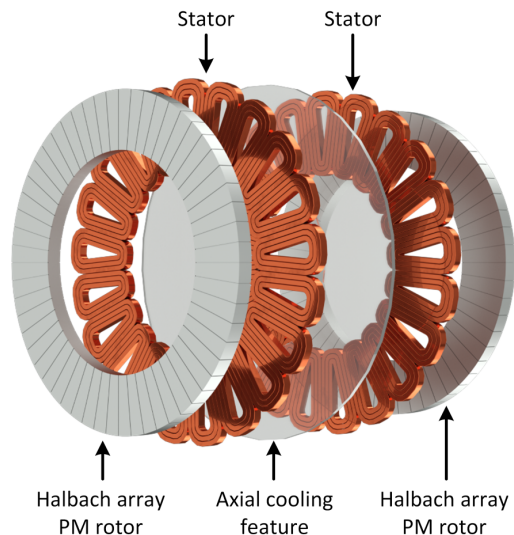


Fig. 22. A coreless AFPM with Halbach array rotors, two stators, and an integrated cooling feature based on the concept proposed in [25].

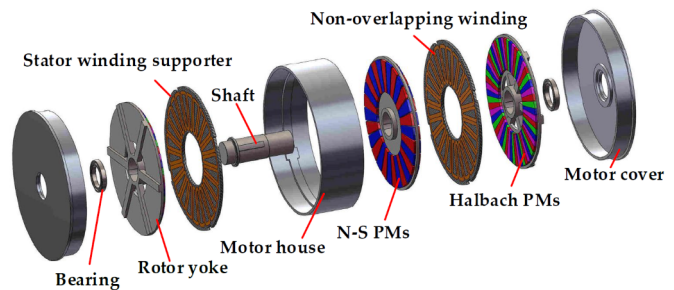


Fig. 23. A coreless AFPM machine of the MSMR type with Halbach array outer rotors and a conventional PM array for the coreless inner rotor [85].

array configuration where the normally magnetized PMs are wider than the tangential ones, torque generation may or may not exceed that of a machine using a conventional Halbach array. The torque produced depends on the width of the coil sides, which is influenced primarily by the pole-to-coil number ratios and the machine's diameter. This relationship is illustrated in Fig. 21, which shows the flux density for varying normal PM widths at a constant pole pitch for an example double-sided Halbach array. The simulated air gap flux densities indicate that a wider flux density window, resulting from increased normal PM width, overlaps a larger portion of the coil sides, potentially enhancing torque production. The simultaneous reduction in flux density amplitude may counteract this benefit. The interplay between these two opposing effects determines the overall torque production change.

The performance comparison between the Halbach PM array and surface-mounted PM rotors was discussed earlier in this subsection. Additionally, Wang *et al.* [62] compared the performance of coreless AFPM machines equipped with Halbach PM array and spoke rotors. Their findings indicate that the machine with the Halbach PM rotor variant delivers nearly 30% higher torque than a similarly sized spoke rotor. Furthermore, due to the higher magnetic loading provided by

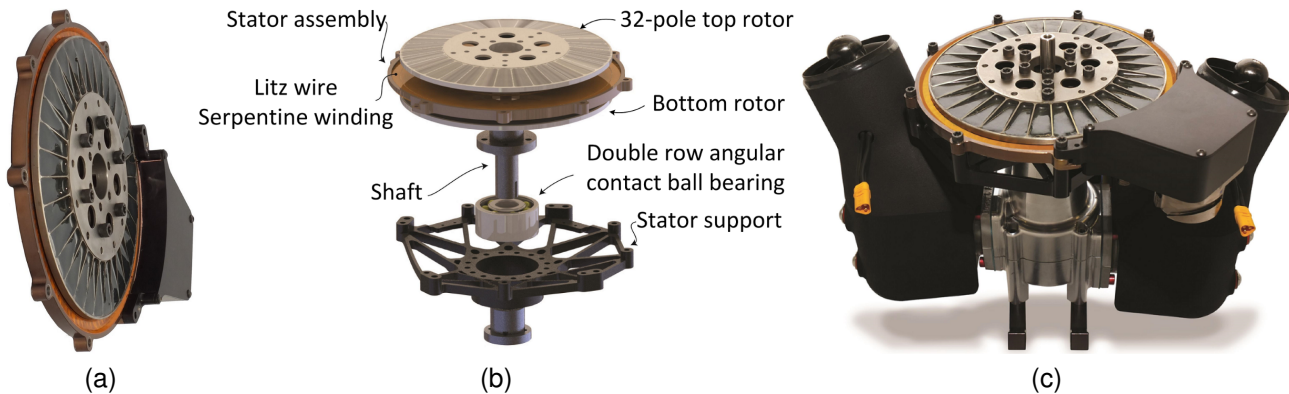


Fig. 24. An example of a fully coreless AFPM machine for aerospace applications, showing (a) a compact view of the machine, (b) an exploded view with mechanical parts, and (c) an assembled engine and coreless AFPM generator. Photo courtesy of LaunchPoint Electric Propulsion Solutions, California, U.S. [156]–[159].

the Halbach rotor, it achieves greater efficiency when both machines generate the same power.

Coreless AFPM machines with a Halbach PM array rotor have been proposed in the literature for various applications, some of which are reviewed below. Mecrow *et al.* [42], [43] developed and optimized such a machine for an in-wheel, solar-powered electric vehicle. Their optimized motor achieved an efficiency of 97.5% and a mass of 8.3 kg, significantly outperforming other brushless DC motor technologies available at the time, which had efficiencies ranging from 92% to 95% and masses between 12 to 16 kg.

Another application is in wind turbine generators, where the high efficiency, zero torque ripple, and lightweight construction of coreless AFPM machines, combined with the size and mass reduction offered by Halbach rotors, make them ideal for direct-drive wind turbines. For instance, Subotic *et al.* [112], [114] conducted a multiphysics design study for a coreless AFPM generator with a Halbach PM rotor for airborne wind turbines. Similarly, Ubani *et al.* [152] and Vatani *et al.* [21] investigated coreless AFPM generators with Halbach PM rotors for direct-drive wind turbine applications.

The applications discussed are highly cost-sensitive, making the use of Halbach PM arrays potentially impractical. The most promising application for coreless AFPM machines with Halbach PM array rotors is potentially in electric aircraft propulsion systems, where the cost can be justified by the stringent requirements for electric motors and the comparatively high overall cost of an aircraft. This type of machine has been explored in research projects funded by the National Aeronautics and Space Administration (NASA), as reported in [25], [160], [161]. The concept featuring a Halbach PM rotor proposed in [25], shown in Fig. 22, incorporates direct axial cooling to enable high current density levels.

Multi-stator and multi-rotor (MSMR) coreless AFPM machines with Halbach PM array rotors, as illustrated in Fig. 23, have also been proposed for electric aircraft propulsion systems. In this configuration, the outer rotors use Halbach arrays, while the middle rotor(s) consist of conventionally magnetized PMs with alternating polarity mounted in a non-ferromagnetic material. As discussed in [33], the MSMR

topology can enhance specific power compared to the single-stator and double-rotor (SSDR) topology and also provides higher fault tolerance.

An example of the application of coreless AFPM machines with Halbach PM array rotors in the aviation industry can be found in the products of LaunchPoint Electric Propulsion Solutions, as shown in Fig. 24. The engine and coreless AFPM motor in Fig. 24c roughly produce the same power, while the coreless AFPM is significantly lighter and smaller. They developed a unique Halbach PM array with four PMs per wavelength, in which the tangentially magnetized PMs are divided into three sections, with the middle section replaced by non-ferromagnetic material [156]. Although this configuration may slightly increase leakage flux from the side not facing the air gap, it significantly enhances mechanical robustness.

VI. ELECTROMAGNETIC MODELING

Axial flux machines present complex 3D electromagnetic problems due to two effects: the radial dependency of flux distribution and the fringing fluxes at the outer and inner radii [1]. The radial dependency in the rotor and stator causes varying flux distributions across different radii, commonly referred to as the curvature effect. Additionally, the fringing flux, or edge effect, particularly exists at the outer and inner radius of axial flux machines. This issue is even more severe in coreless stator AFPM machines due to the larger air-gap and the absence of a stator core.

One method for accelerating the modeling of AFPM machines is the use of equivalent 2D electromagnetic analytical or numerical methods. The simplest 2D model involves cutting the 3D model at the mean radius and unfolding it to create an equivalent 2D linear model. This technique can be integrated into FEA modeling and further expedited by applying matching and symmetry boundary conditions. However, this type of modeling neglects curvature and edge effects, which reduces calculation accuracy. The influence of curvature effect in pole widths and coil side distributions across three 2D planes at varying radii in a coreless AFPM machine is depicted in Fig. 25. As the cutting plane radius approaches the machine's outer radius, both the pole width and the distance between coil sides

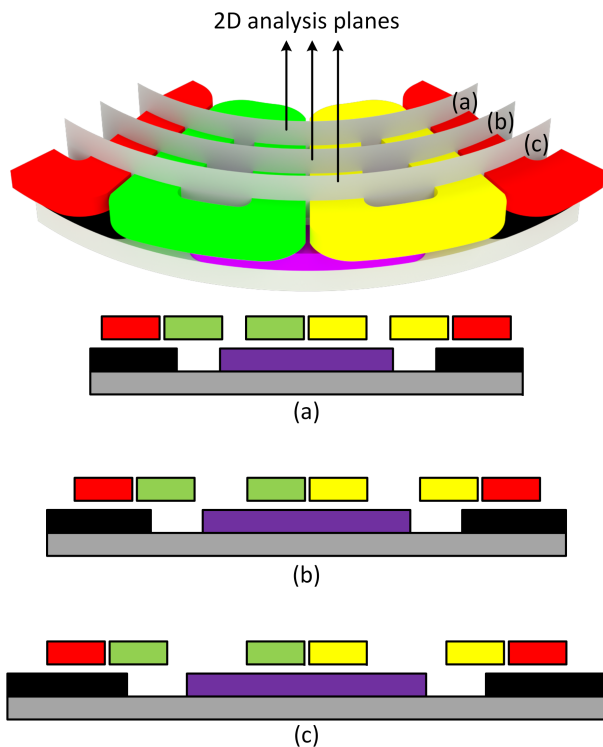


Fig. 25. A diagram illustrating a method to calculate the field in AFPM machines using the selected 2D analysis planes for unrolling different radii based on the method proposed by Eastham *et al.* [162].

increase. This leads to distinct flux distributions in different cut planes of the original model.

To enhance the accuracy of the equivalent 2D model by incorporating the curvature effect in AFPM machines, Eastham *et al.* [24], [162] proposed cutting the 3D model at several radii, forming cylindrical surfaces, and unrolling each to create multiple equivalent 2D linear models. The final solution is then obtained by superimposing the results from each slice. Gulec *et al.* [163] further explored the modeling of various AFPM machines using three types of 2D models: linear, inner rotor radial, and outer rotor radial models. Their comparative analysis revealed that coreless AFPM machines could be accurately modeled using a few 2D models at different radii, employing either inner rotor, outer rotor, or linear approaches.

While the curvature effect in coreless and slotless AFPM machines is similar to that of conventional cored counterparts, the edge effect is generally more pronounced and requires careful consideration in 2D modeling. For instance, Bumby *et al.* [164] presented an analytical model of a slotless AFPM machine using an equivalent 2D model at the mean radius. To account for the significant fringing flux at the outer and inner radii, they introduced a coefficient to compensate for the edge effect in the 2D model. More examples of 2D and quasi-3D modeling of coreless AFPM machines can be found in [130], [165]–[168]. These studies consistently indicate that 2D modeling is well-suited for performance evaluation and the early stages of the design process.

To accurately consider curvature and edge effects for detailed simulations in the final stages of design, 3D modeling

is essential. While 3D FEA provides the most precise results, it entails significant computational burdens. To mitigate this, two main approaches are found in the literature: ultra-fast FEA techniques and 3D analytical modeling.

There is a growing need for ultrafast 3D FEA models for AFPM machines that support performance analysis, extensive parametric studies, and design optimizations. Out of the surveyed literature, foundational work on ultrafast FE models was found in [169] and [170] with very recent examples including one for coreless AFPM machines [171]. This model leverages the geometric symmetry in the machine's topology and employs a systematic approach to determine the minimal number of transient FE solutions necessary for torque prediction.

Three-dimensional analytical methods, although less accurate, offer much faster computation times. This makes them ideal for preliminary design phases where quick evaluations are crucial [172], [173]. The conventional analytical approach for modeling coreless AFPM machines employs subdomain modeling to determine the air-gap flux density generated by the rotors. This flux density is then combined with the winding factor and the Lorentz force theorem to compute the resulting torque. Several studies utilizing this approach can be found in [130], [174]–[176]. Other well-established methods, such as conformal mapping, can also be utilized for modeling coreless AFPM machines due to the absence of ferromagnetic material.

Another method for analytically modeling coreless stator AFPM machines is the magnetic equivalent circuit (MEC) technique, which offers faster but less accurate results compared to 3D FEA. The primary challenge in MEC modeling of electric machines lies in accurately predicting flux distribution, particularly in the air-gap, which is highly dependent on the machine's dimensions and rotor positions [177]. Zhang *et al.* [178] and Zhao *et al.* [179] presented MEC models for coreless AFPM machines that showed good agreement with 3D FEA results and experimental measurements.

While these studies validated the MEC models for a few specific designs, other references in the literature, such as those by Ding *et al.* [180], Aydin *et al.* [181], and Daghigh *et al.* [182], have employed MEC models for design optimization. These studies indicated that designs selected through MEC-based optimization can achieve performances comparable to those obtained through 3D FEA.

VII. POWER LOSSES

Electromagnetic losses in coreless stator AFPM machines primarily include Joule and eddy current losses in the conductors and PMs. The absence of electrical steel in the stator eliminates eddy current and hysteresis losses typically associated with stator cores. Additionally, eddy current core losses in the rotor back iron are generally negligible due to the low amplitudes of harmonic fields produced by the stator.

In coreless stator AFPM machines, the stator windings are directly exposed to the rotating flux generated by the PMs, as there are no stator teeth to shield them. This direct exposure induces alternating eddy currents in the stator conductors, resulting in losses. Within the air-gap, both tangential and normal magnetic flux density components are present. The

normal component induces eddy currents across the width of the conductor, while the tangential component induces eddy currents in the depth of a conductor [4]. These eddy current losses can become significant at relatively high speeds and frequencies, leading to increased temperatures and a reduction in the machine's efficiency [183].

Accurate calculation of eddy current in coreless stator AFPM machine requires modeling every single planar conductor with 3D FEA, leading to a considerable computation burden and being highly time-consuming. A common approach to reducing these memory-intensive calculations is to model only a fraction of the machine and its coils while applying appropriate boundary conditions. The results are then extrapolated to estimate eddy current losses in the unsimulated coils. Another well-known method is to calculate the flux density through 2/3D FEA and feed that into analytical equations to calculate the eddy current losses [183]–[185].

The eddy current losses in the conductors of a coreless or slotless stator AFPM machine are influenced by the conductor's cross-sectional geometry, the amplitude of the flux density it encounters, and the operating frequency. For conductors with a rectangular cross-section, the total eddy current losses can be determined from [185]:

$$P_{ed} = \frac{\pi^2 N_c N_t f^2 t_w t_h l_c}{3\rho} (t_w^2 B_z^2 + t_h^2 B_\phi^2), \quad (8)$$

where N_c represents the number of coils with an average length l_c , and N_t denotes the number of turns per coil. The variables B_z and B_ϕ correspond to the axial and tangential components of the flux density, respectively. Additionally, t_w is the trace width, t_h is the trace height, and f is the frequency. This relationship indicates that eddy current losses increase proportionally with the cube of the trace width and height.

A well-known method for reducing stator eddy current losses is to design the machine with smaller conductor cross-sections using multiple parallel paths or Litz wires. While Litz wires can significantly reduce conductor eddy current losses, they are more expensive than conventional conductors or PCB stators. To minimize eddy current losses in stators made of conventional wire or PCB, multiple parallel conductors with small cross-sections must be employed.

However, using multiple parallel paths introduces another type of loss in the conductors. Since the parallel conductors are at varying distances from the rotor surface, each layer experiences different flux density levels, leading to higher induced EMFs in the conductors closer to the magnets than those farther away. This difference in potential between conductors can result in circulating currents among the parallel layers, causing additional losses. To minimize these circulating eddy currents, the induced EMFs in all parallel layers must be equalized through conductor transposition or twisting techniques.

Reducing eddy current losses by selecting a thinner cross-section conductor may lead to an increase in Joule losses due to the higher resistance. Achieving an optimal balance between eddy current and Joule losses requires careful selection of the wire size at the rated speed of the coreless stator AFPM machines [186], [187].

Due to the trend and the benefits PCB stators offer to core-

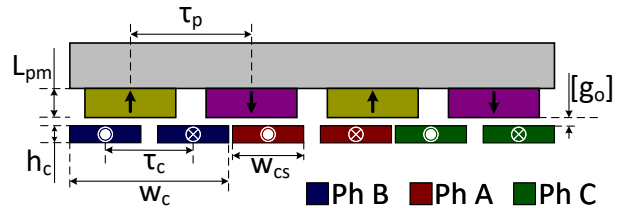


Fig. 26. Winding geometrical parameters for half of a SSDR machine of the concentrated winding topology where $\tau_c = \frac{4}{3}\tau_p$. The second rotor is omitted for clarity.

less stator AFPM machines, numerous previous publications have studied the eddy current within PCB stator machines considering the existing technology in PCB production. These papers have considered the size and limitation in traces' cross-section geometry to minimize eddy current and the availability of the number of stacked layers to decrease the circulating losses. For example, Francois *et al.* [188] proposed adding slits along the conductive traces to mitigate eddy current losses and Chulaee *et al.* [18], [26] mitigated both eddy current and circulating losses by employing multi-layer PCB technology to design a stator with multiple parallel paths and transposing the conductors across the PCB layers.

Another type of electromagnetic loss that may be observed in coreless AFPM machines is eddy current loss in the PMs. Due to the high conductivity of NdFeB magnets, they are prone to induced eddy currents and associated losses. Typically, these losses can be neglected in coreless stator AFPM machines because of the low harmonic flux produced by the stator and the large air-gap [187]. However, in heavily loaded machines and at relatively high rotor speeds, eddy current losses in the magnets can become significant, leading to increased temperatures and the potential for permanent demagnetization of magnets.

The literature lacks studies specifically addressing eddy current losses in the magnets of coreless stator AFPM machines since these losses are insignificant except in very specific cases involving heavy loads and high-speed operation. Nevertheless, methods used in AFPM machines with iron-cored stators to reduce eddy current losses in the magnets can also be applied to coreless stator designs. A well-known approach is to use segmented PMs rather than a uniform magnet [189], [190].

VIII. DESIGN AND SIZING

This section details a preliminary design procedure and sizing evaluation for coreless stator AFPM machines, leveraging analytical calculations of torque and back electromotive force (B-EMF). Given specified parameters such as outer diameter, torque, speed, and efficiency, this design approach facilitates the estimation of critical geometric and electromagnetic characteristics. The equations developed are derived from the 2D modeling of AFPM machines at arbitrary diameters, allowing for the use of either single or multiple radial cuts in the 2D modeling process. These equations are general and can be applied to various winding and rotor configurations.

In coreless stator machines, force generation derives from the interaction between the magnetic flux density of the perma-

TABLE I
POSSIBLE COMBINATIONS OF COIL-TO-POLE NUMBER RATIOS FOR
CONCENTRATED WINDINGS IN CORELESS AFPM MACHINES, ALONG WITH
THEIR CORRESPONDING SYMMETRY COEFFICIENT, NUMBER OF COILS,
AND THE COEFFICIENT K_1 USED IN THE TORQUE EQUATION.

| Coil to pole ratio | Analysis frac. coeff. (K_s) | N_c | K_1 |
|-----------------------|------------------------------------|------------------|----------------|
| 3/2 | $\frac{P}{2}$ | $\frac{3P}{2}$ | $\frac{3}{8}$ |
| 3/4 | $\frac{P}{4}$ | $\frac{3P}{4}$ | $\frac{3}{16}$ |
| 9/8 | $\frac{9P}{8}$ | $\frac{9P}{8}$ | $\frac{9}{32}$ |
| 9/10 | $\frac{9P}{10}$ | $\frac{9P}{10}$ | $\frac{9}{40}$ |
| 12/10 | $\frac{12P}{5}$ | $\frac{12P}{10}$ | $\frac{3}{20}$ |
| 12/14 | $\frac{12P}{7}$ | $\frac{12P}{14}$ | $\frac{3}{28}$ |

ment magnets, B_n , and the current density in the conductors, J . This interaction, known as the Lorentz force, can be described by [191]:

$$F = \int_V \vec{J} \times \vec{B} dV, \quad (9)$$

where B can be calculated through (3) and (7) for surface PM and Halbach rotors, and J can be derived from:

$$J = \frac{N_t I_p k_w}{h_c w_c}. \quad (10)$$

The number of turns per coil is denoted by N_t , I_p represents the peak current, h_c and w_c are the axial length and side width of the coil respectively, as illustrated in Fig. 26, and k_w is the winding factor.

To calculate the single phase maximum tangential component of force, the normal component of flux density, together with the current in the Z-directed conductor must be inserted in 9, resulting in:

$$F_{max}(x, i) = N_t I_p k_w B_1 D_{ro} \frac{\lambda - 1}{2\lambda}, \quad (11)$$

where B_1 is the peak value of flux density fundamental component, which can be calculated using (3) and (7) when $i = 0$, D_{ro} is the rotor's outer diameter, and λ is the ratio of the rotor's outer diameter to its inner diameter, defined as $\lambda = \frac{D_{ro}}{D_{ri}}$.

The average torque for a three-phase machine at an arbitrary diameter can be determined by multiplying equation (11) by the matching boundary coefficient, the arbitrary radius, and a factor of $\frac{3}{2}$. In this paper, the torque equation is derived at the average diameter, as numerous studies, including [130], have indicated that analytical torque equations at this diameter show good agreement with results from 3D FEA.

$$T_{avg} = K_1 N_t I_p k_w B_1 P D_{ro}^2 \frac{\lambda^2 - 1}{8\lambda^2}, \quad (12)$$

where P denotes the number of poles, and K_1 is a constant that depends on the fraction of the total model to be analyzed and the radius at which the torque is calculated. The values of the coefficient K_1 for different coil-to-pole number ratios are provided in Table I. For coreless stator machines utilizing Neodymium Iron Boron (NdFeB) magnets, the peak air-gap

flux density typically ranges from 0.5 T to 0.7 T for surface PM rotors and from 0.7 T to 1.0 T for Halbach array rotors, depending on the rotor design, PM grade, and M2M gap.

The rotor diameter ratio, λ , is one of the key design variables in coreless stator AFPM machines, exerting a notable influence on machine characteristics. The optimal selection of λ highly depends on the design objectives and varies across different rated powers, pole pairs, and materials [13].

When choosing a value for λ for the surface PM rotor variant, it is essential to account for the saturation of the back iron. In AFPM machines, the radius effect causes the flux density in the backing iron to be greater at the outer radius than the inner radius. This difference can lead to varying saturation levels in the back iron core at different radii. In the case of the Halbach rotor configuration, the impact of λ becomes even more significant. It was shown that for rotor radial lengths exceeding one pole pitch, the generated power does not increase proportionally with the rise in λ [21], [25].

The number of turns can be determined from the B-EMF equation, and the phase voltage supplied by the power electronic and drive systems. The peak value of B-EMF can be expressed as:

$$E = K_2 N_t B_1 k_w n_s D_{ro}^2 \frac{\lambda^2 - 1}{\lambda^2}, \quad (13)$$

where K_2 is a constant with a value of $\frac{\pi}{240}$ and n_s represents the synchronous speed in rpm.

The winding factor is determined by multiplying the coil pitch, k_p , by the distribution factors in both the X- and Y-directions, k_{dx} and k_{dy} . In contrast to slotted windings, coreless windings require an additional distribution factor in the Y-direction. This is because conductors located further from the PM surface experience a lower flux density. Detailed calculations for the winding factor in coreless stator machines were outlined in [102]. The fundamental component of the winding factor, which depends on the coil and rotor geometries, can be calculated as:

$$k_w = k_p \cdot k_{dx} \cdot k_{dy} \quad (14)$$

$$k_p = \sin\left(\frac{\pi(1 - K_3)}{N_c}\right) \quad (15)$$

$$k_{dx} = \frac{N_c}{\pi K_3 K_s} \sin\left(\frac{\pi K_3 K_s}{N_c}\right) \quad (16)$$

$$k_{dy} = \frac{2\tau_p}{\pi h_c} \tanh\left(\frac{\pi h_c}{2\tau_p}\right), \quad (17)$$

where $K_3 = \frac{w_{cs}}{\tau_c}$, K_s is the analysis fraction coefficient that can be determined based on Table I, τ_c and τ_p denote the coil and pole pitches, w_{cs} and h_c are the width and axial length of the coil side, and w_c represents coil width. The coil and rotor geometries are defined in Fig. 26 for an example coil-to-pole ratio of 3/4.

Based on the required efficiency and rated power, the power loss can be estimated. The primary electromagnetic losses in coreless AFPM machines are copper and stator eddy current losses. Typically, if appropriate Litz wire or a PCB stator with fine conductor transposition is used, stator eddy current losses

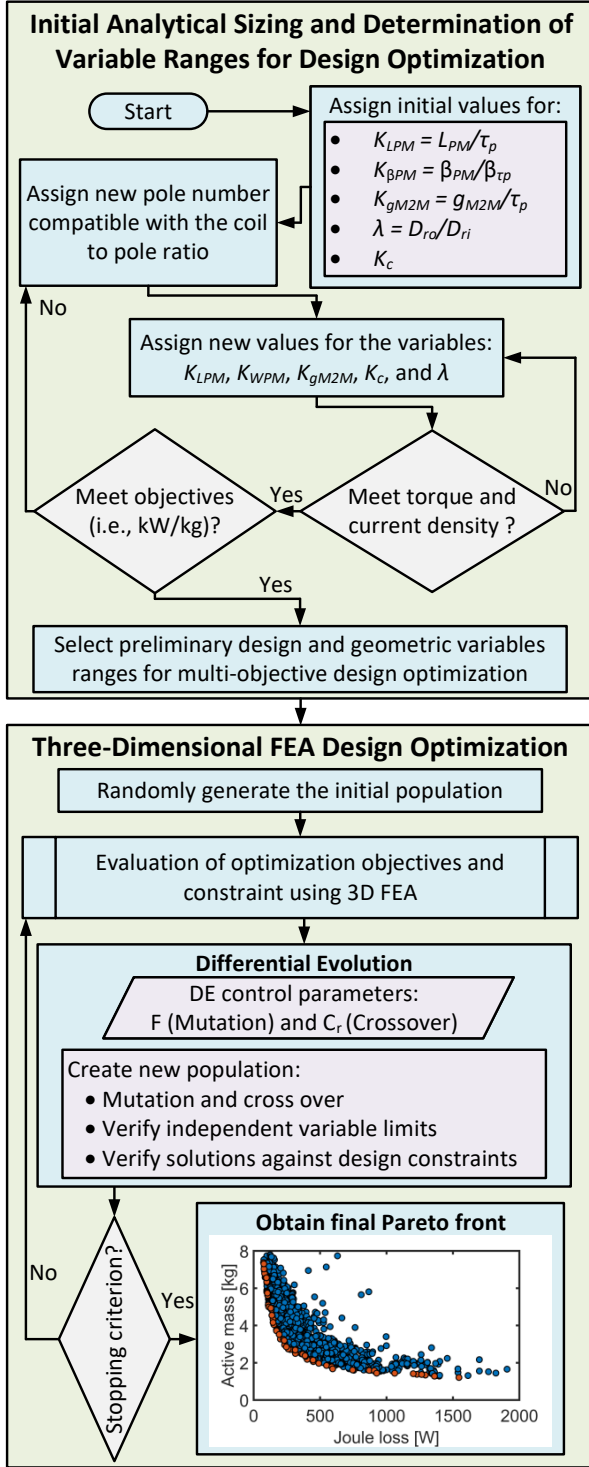


Fig. 27. The proposed hybrid analytical and FEA design process for coreless stator AFPM machines.

amount to 15% to 20% of the copper losses. Therefore, from the estimated copper losses, the peak current value can be calculated using:

$$I_p = \sqrt{\frac{2P_{Cu}}{3R_{Ph}}}, \quad (18)$$

where P_{Cu} represents the total copper loss and R_{Ph} is the

phase resistance, which can be calculated using:

$$R_{Ph} = \frac{\rho N_c N_t (2\ell + \ell_{ue} + \ell_{le})}{h_c w_c k_f}, \quad (19)$$

where ρ is the resistivity of copper, N_c is the coil number that can be determined based on the Table I, k_f is the copper fill factor, and w_c and h_c are the width and axial height of the coil sides. The lengths ℓ , ℓ_{ue} , and ℓ_{le} represent the active length, the upper end winding length, and the lower end winding length of the coils, respectively, and can be calculated using:

$$\ell = D_{ro} \left(\frac{\lambda - 1}{2\lambda} \right) + w_c (2k_c - 1) \quad (20)$$

$$\ell_{ue} = \frac{\pi}{N_c} [D_{ro} + w_c (2k_c - 1)] \quad (21)$$

$$\ell_{le} = \frac{\pi}{N_c} \left[\frac{D_{ro}}{\lambda} + w_c (1 - 2k_c) \right]. \quad (22)$$

The coefficient k_c , which varies between 0 and 1, determines the active length of the stator coils by adjusting the stator's outer diameter as:

$$D_{so} = D_{ro} + 2k_c w_c. \quad (23)$$

The impact of k_c has been explored in [18], suggesting that $k_c = 1$ results in minimal PM usage, $k_c = 0$ leads to the highest power losses, and $k_c = 0.5$ offers a balanced compromise between PM mass and efficiency.

Based on the presented analytical modeling, 3D FEA, and an evolutionary optimization algorithm, a systematic design process is proposed and illustrated as a flowchart in Fig. 27. Given the required power, speed, efficiency, outer diameter, and cooling conditions—which determine the allowable current density—the flowchart outlines a structured approach to designing the machine for a specific application. The proposed optimization methodology comprises two sequential stages. In the first stage, an initial sizing procedure using fast analytical modeling is conducted to establish the preliminary design of the machine and define the variable ranges for the subsequent optimization process. In the second stage, 3D FEA models are used within an evolutionary optimization algorithm to explore the design space and identify the Pareto front.

The design process assumes a fixed coil-to-pole ratio, allowing it to be iterated multiple times for different ratios to determine the optimal ratio. The geometric design variables are normalized as follows: PM length and magnet-to-magnet gap are normalized based on the pole pitch width at the radius where the calculations are being conducted; pole arc is normalized based on the pole pitch angle ($\frac{2\pi}{P}$); the inner diameter is normalized relative to the outer diameter; and K_c is defined as a fraction of coil width, changing between 0 and 1. This normalization system is chosen based on the analytical equations developed for flux density and torque calculations.

The design process begins by assigning initial values to all geometric variables. The phase resistance is then calculated, allowing the determination of the maximum phase current based on the required efficiency. Next, the flux density, winding factors, and torque are computed. The winding factors are determined using the equations 14 to 17 and the following

TABLE II
PERFORMANCE CHARACTERISTICS OF EXAMPLE PM MACHINES DESIGNED FOR ELECTRIC AIRCRAFT PROPULSION. VALUES REPORTED IN PARENTHESIS
CONSIDER ONLY THE ELECTROMAGNETIC ACTIVE COMPONENTS.

| Ref. | Year | Flux pattern | Structure | Power [kW] | Speed [rpm] | OD [mm] | Spec. PWR [kW/kg] | Spec. TRQ [N.m/kg] | Eff. [%] | Current dens. [A/mm ²] | Cooling |
|-------|------|--------------|-------------------|------------|-------------|---------|-------------------|--------------------|----------|------------------------------------|-------------|
| [43] | 1999 | AFPM | Coreless, SPM | 1.80 | 1,060 | 360 | 0.2 | 0.002 | 97.4 | 3.12 | Natural |
| [43] | 1999 | AFPM | Coreless, Halbach | 1.80 | 1,060 | 360 | 0.2 | 0.002 | 98.2 | 2.47 | Natural |
| [24] | 2001 | AFPM | Coreless, SPM | 2.25 | 1,000 | 280 | 0.5 | 0.005 | 94.7 | 4.8 | Natural |
| [50] | - | AFPM | Coreless, Halbach | 5.20 | 8,400 | 152 | 8.2 | 0.01 | 95.0 | - | Natural |
| [50] | - | AFPM | Coreless, Halbach | 112 | 3,500 | 457 | 7.5 | 0.02 | 97.0 | - | Natural |
| [193] | 2022 | AF/RFPM | Slotless, Halbach | 250 | 5,000 | - | 8.0 (29.9) | 57.1 | 97.0 | 29.0 | Refrigerant |
| [189] | 2022 | AFPM | YASA, Halbach | 250 | 5,000 | 270 | (33.3) | 63.7 | 94.0 | 35.6 | Water |

coil geometry equations: $W_c = \frac{\pi D}{N_c}$, $W_{cs} = \frac{\pi D_{ri}}{N_c}$, and $h_c = g_{M2M} - 2l_g$.

At this stage, the evaluated design must be checked to ensure it is within an acceptable range of the rated power and allowable current density, which is decided by the machine's cooling conditions. If the design does not meet these requirements, new geometric variables—except for the pole number—are assigned, and the process is repeated.

In the subsequent step, the design is evaluated against specific objectives such as required specific power, power density, cost, and other performance criteria. If the design fails to fall into an acceptable range for the objectives, the pole number is changed, and the previous stage is repeated. This iterative process continues until a preliminary design is established, along with variable limits that satisfy both the required torque and current density while meeting the predefined objectives.

In the second stage, the 3D FEA parametric model of the machine is coupled with an evolutionary optimization method to explore the variable ranges identified in the first stage and to determine the optimal Pareto front accurately. The algorithm generates an initial population of random designs and iteratively refines them over successive generations until the stopping criteria are met. The final design is typically chosen from the knee region of the Pareto front, where an optimal balance between competing objectives is achieved. A comprehensive discussion of electric machine optimization and effective evolutionary methods for this application can be found in [192].

IX. REVIEW OF RECENT AND RELEVANT ADVANCES IN ELECTRIC AIRCRAFT PROPULSION TECHNOLOGY

This paper has reviewed extensively surveyed coreless stator AFPM machines from topological, material, and electromagnetic performance and design perspectives. This section discusses several examples of recent projects and publications on electric aircraft propulsion technologies using AFPM motors with coreless stators. Coreless AFPM machines have also been proposed and studied for propulsion systems that do not necessarily require constant power operation over a wide speed range, such as solar cars [23], [43] and e-bikes [194]. Due to the relatively low phase inductance and consequently

reduced performance of coreless AFPM machines under flux-weakening conditions [122], [195] compared to conventional cored machines, their use in electric vehicle powertrains is somewhat constrained.

As specified in the introduction, this paper focuses on machines operating at higher than ambient temperatures. The current review does not include machines operating at very low temperatures, such as those specific to cryogenic applications and superconducting machines, some of which may also employ coreless axial flux topologies and PMs in their special implementations, e.g. [196], [197].

The aviation industry is currently responsible for approximately 3% of global CO₂ emissions, but, most importantly, according to a forecast by Roland Berger [198], this figure could increase to 24% by 2050 if other sectors decarbonize as expected and no significant technological breakthroughs occur in conventional propulsion systems. Current electric powertrains require advancements in both power density and efficiency to facilitate the realization of fully decarbonized aviation. Examples of recent and ongoing projects include those from the US Department of Energy ARPA-e ASCEND program [199] and NASA Integrated Zero-Emission Aviation (IZEA) University Leadership Initiative (ULI) [200]. Ultra-high performance benchmarks for a fully integrated all-electric powertrain with a minimum power density of 12 kW/kg and an efficiency above 93%, demonstrated at a typical 250kW at 5,000rpm, have been studied through multiple ASCEND projects, including the examples outlined in the following.

An axial flux yokeless and segmented armature (YASA) machine with two Halbach PM array rotors and an integrated cooling system was proposed and developed by Talebi *et al.* [189]. The machine employs a six-phase winding with a very high slot fill factor and operates at a very high current density. The Halbach array-oriented PMs are segmented radially to reduce rotor eddy current losses and are mounted on a carbon fiber backplate. The stator segments are made of grain-oriented electrical steel for higher permeability and reduced core losses. The thermal management system incorporates mini-channel heatsinks attached to the end windings at the outer edge and a circulating water ethylene glycol cooling system to dissipate heat from the heatsinks. This machine has a calculated active specific power for electromagnetic components of 33 kW/kg and an efficiency of 94% [201].

A special 3D rotor with two radial and one axial air-gap surfaces for electromagnetic torque production was proposed and developed by Du *et al.* [193]. The machine's stator features a concentrated slotless winding made of Litz wire wound around a laminated cobalt iron circular core with an I-shaped cross-section. In order to leverage the end winding for torque production, a D-shaped core composed of soft magnetic composite is incorporated at the bending radius between the end windings and the I-shaped stator core. The three rotor sections employ Halbach PM arrangements, with the axial part contributing significantly more to the torque than the radial ones. An additively manufactured heat exchanger with parts separating the coils and internal micro-channels for circulating dielectric refrigerant coolant, summarized in the Table I as refrigerant, is designed for stator cooling, enabling high current density of larger than 20 A/mm^2 [202]. This motor has active specific power for electromagnetic components higher than 29 kW/kg and a total specific power, including all components, of 8 kW/kg . The efficiency at rated torque and speed is reported as 93.4% [203]

A third example of high power, specific power, and efficiency machine for electric aircraft was proposed and developed by Mason *et al.* [204]. In this case, the topology is of the radial type, but nevertheless the motor is included in the review as is of the coreless type, which is possible due to the use of inner and outer rotors with Halbach PM arrays, and also employs Litz wire and special highly effective direct liquid cooling. It is noted that the rotor is based on a novel PM-wire technology, consisting of a single-piece, ring and helix Halbach array with continuously varying magnetization. This approach eliminates the need for a rotor back iron, simplifies manufacturing, and enhances robustness compared to conventional Halbach rotors. Its cooling system relies on immersing the stator coils in a circulating water-glycol coolant to dissipate heat efficiently. Experimental tests have demonstrated that this motor can operate at an extremely high current density of approximately 60 A/mm^2 . The machine was reported to achieve the electromagnetic and total power density of 26 and 11.9 kW/kg , respectively, and 94.5% rated efficiency [205].

The mechanical design of motor envelopes should also be optimized to enhance the specific power density of AFPM machines. For example, unlike radial flux machines, axial flux machines lack a stator that can serve as a protective barrier in the event of a rotor burst. The aluminum housing used in these machines may require reinforcement or be thicker than that of the radial flux machine for safety; however, increasing its thickness would negatively impact specific power density.

The example AFPM machines compiled in Table II illustrate power rating increase and performance improvements over the years, benefiting from a combination of design, electromagnetic, mechanical and thermal advancements. This progress can be further enhanced by employing advanced cooling techniques, such as cryogenic cooling, and utilizing higher-density materials like aluminum for windings. A study by Manolopoulos *et al.* [206] demonstrated that at cryogenic temperatures, the electrical resistivity of aluminum becomes lower than that of copper. Since aluminum has a density nearly three times lower than copper at room temperature, employing

aluminum Litz wire combined with cryogenic cooling may significantly improve specific power density.

X. CONCLUSION

This paper provided an independent review of the many concepts and developments of axial flux permanent magnet machines with coreless stators, including recent advancements. The review reflects the authors' many decades of cumulative experience on the subject matter and the contributions by many other professional colleagues. These have been acknowledged and cited in the list of references, which includes 187 references. The topic continues to be of great timely interest, including applications for electric propulsion. The following is a short summary of the sections presented in this paper.

- **Topologies:** Various topologies of coreless AFPM machines in the literature are reviewed that identify double-rotor and single-stator as the most dominant types. Multi-stators and multi-rotors were used whenever high power was required in a fixed diameter. Single stator and single rotor topology are not very popular because of low magnetic loading, but they can be used with much higher current loading since the topology allows the employment of effective cooling systems.
- **Winding:** Winding topologies and materials within AFPM machines with coreless stator types are reviewed, which indicates the recent trend in employing concentrated winding rather than overlapping due to the more straightforward manufacturing and design. Special attention is given to reviewing publications that employ printed circuit board (PCB) coreless stators that benefit from high reliability, mass production capability, and low cost from the manufacturing perspective.
- **Rotor:** Rotor configurations proposed in the literature for coreless AFPM machines include surface-mounted, spoke, and Halbach array PM, of which the surface-mounted is the most popular. Halbach array PM rotors can significantly improve the torque density of the machine in a constant envelope, at the disadvantage of being more expensive and having manufacturing complexity.
- **Electromagnetic modeling:** Electromagnetic methods presented for coreless AFPM machines in the literature and the methods that have been studied for cored AFPMs but applicable to the coreless type were reviewed. One contribution to reducing the computation burden of 3D electromagnetic problems for either cored or coreless type AFPM machines, is using equivalent 2D modeling with the cost of lower accuracy. Different approaches are reviewed, indicating that for preliminary design steps, 2D numerical or analytical approaches are acceptable, but accurate assessment needs 3D finite element analysis to consider the curvature and edge effects.
- **Power losses and mitigating methods:** Existing electromagnetic power losses in coreless AFPM machines were identified, showing that copper and eddy and circulating current losses are the most dominant. It can be concluded from the reviewed literature that to mitigate eddy current and copper losses, a trade-off between conductor sizes is

needed and that transposition between layers of windings helps reduce circulating losses.

- **Design and sizing:** A design procedure for coreless AFPM machines was established based on equivalent 2D modeling. This procedure can be used for the primary estimation of the required electromagnetic and geometric parameters for a specified power output, speed, and efficiency. Additionally, the impact of both electromagnetic and geometric parameters on torque development was discussed.
- **Review of Recent and Relevant Advances in Electric Aircraft Propulsion Technology:** This section reviewed axial and radial flux PM machines proposed and developed over the years as well as very recently for electric aircraft propulsion. The focus was on configurations of the axial flux type and/or with coreless stators.

XI. ACKNOWLEDGMENT

The material is based upon work supported by the National Aeronautics and Space Administration (NASA) through the University Leadership Initiative (ULI) #80NSSC22M0068 and by the National Science Foundation (NSF) through a Graduate Research Fellowship under Grant No. 2239063. Any findings and conclusions expressed herein are those of the authors and do not necessarily reflect the views of the sponsor organizations.

REFERENCES

- [1] F. Giulii Capponi, G. De Donato, and F. Caricchi, "Recent advances in axial-flux permanent-magnet machine technology," *IEEE Transactions on Industry Applications*, vol. 48, no. 6, pp. 2190–2205, 2012.
- [2] S. Huang, J. Luo, F. Leonardi, and T. Lipo, "A comparison of power density for axial flux machines based on general purpose sizing equations," *IEEE Transactions on Energy Conversion*, vol. 14, no. 2, pp. 185–192, 1999.
- [3] F. Nishanth, J. Van Verdegheem, and E. L. Severson, "A review of axial flux permanent magnet machine technology," *IEEE Transactions on Industry Applications*, vol. 59, no. 4, pp. 3920–3933, 2023.
- [4] J. F. Gieras, R.-J. Wang, and M. J. Kamper, *Axial Flux Permanent Magnet Brushless Machines*. Dordrecht: Springer Netherlands Springer e-books, 2008.
- [5] F. Profumo, A. Tenconi, M. Cerchio, J. Eastham, and P. Coles, "Axial flux plastic multi-disc brushless PM motors: performance assessment," in *Nineteenth Annual IEEE Applied Power Electronics Conference and Exposition, 2004. APEC '04.*, vol. 2, 2004, pp. 1117–1123 vol.2.
- [6] C. W. Gabrys and T. S. Rodgers, "Commercial low cost, high efficiency motor-generator," Feb. 15 2011, uS Patent 7,888,839.
- [7] A. Habib, M. A. A. Mohd Zainuri, H. S. Che, A. A. Ibrahim, N. A. Rahim, Z. M. Alaas, and M. M. R. Ahmed, "A systematic review on current research and developments on coreless axial-flux permanent-magnet machines," *IET Electric Power Applications*, vol. 16, no. 10, pp. 1095–1116, 2022. [Online]. Available: <https://ietresearch.onlinelibrary.wiley.com/doi/abs/10.1049/elp2.12218>
- [8] J. Gieras and I. Gieras, "Performance analysis of a coreless permanent magnet brushless motor," in *Conference Record of the 2002 IEEE Industry Applications Conference. 37th IAS Annual Meeting (Cat. No.02CH37344)*, vol. 4, 2002, pp. 2477–2482 vol.4.
- [9] Y. Chulaee, A. Mohammadi, M. Vatani, and D. M. Ionel, "Fault-tolerant axial flux coreless pm machines with independent phase modules," in *2024 IEEE Transportation Electrification Conference and Expo (ITEC)*, 2024, pp. 1–5.
- [10] F. Y. Notash, M. Vatani, J. He, and D. M. Ionel, "Model predictive control of 5l-anpc inverter fed coreless afpm motor with mitigated cmv in electric aircraft propulsion," in *2024 IEEE Energy Conversion Congress and Exposition (ECCE)*, 2024, pp. 1–6.
- [11] M. T. Fard, J. He, H. Huang, and Y. Cao, "Aircraft distributed electric propulsion technologies—a review," *IEEE Transactions on Transportation Electrification*, vol. 8, no. 4, pp. 4067–4090, 2022.
- [12] "Siemens develops world-record electric motor for aircraft," <https://press.siemens.com/global/en/pressrelease/siemens-develops-world-record-electric-motor-aircraft>, Siemens Press, 2025.
- [13] M. Aydin, S. Huang, and T. Lipo, "Axial flux permanent magnet disc machines: A review," *Conf. Record of SPEEDAM*, 01 2004.
- [14] S. Kahourzade, A. Mahmoudi, H. W. Ping, and M. N. Uddin, "A comprehensive review of axial-flux permanent-magnet machines," *Canadian journal of electrical and computer engineering*, vol. 37, no. 1, pp. 19–33, 2014.
- [15] Z. Hao, Y. Ma, P. Wang, G. Luo, and Y. Chen, "A review of axial-flux permanent-magnet motors: Topological structures, design, optimization and control techniques," *Machines*, vol. 10, no. 12, 2022. [Online]. Available: <https://www.mdpi.com/2075-1702/10/12/1178>
- [16] G. Romeo, G. Frulla, E. Cestino, and G. Corsino, "Heliplat: Design, aerodynamic and structural analysis of very-long endurance solar powered stratospheric uav," *AIAA Journal of Aircraft*, vol. 40, no. 6, pp. 1231–1239, November-December 2003.
- [17] Infinitum, "Infinitum, inc." 2025. [Online]. Available: <https://goinfinitum.com/>
- [18] Y. Chulaee, G. Heins, B. Robinson, A. Mohammadi, M. Thiele, D. Patterson, and D. M. Ionel, "Design and optimization of high-efficiency coreless pcb stator axial flux pm machines with minimal eddy and circulating current losses," *IEEE Transactions on Industry Applications*, pp. 1–13, 2024.
- [19] E-Circuit Motors, Inc., "Pcb stator technology electric motors," 2025. [Online]. Available: <https://pcbstator.com/>
- [20] A. S. McDonald, N. Al-Khayat, D. Belshaw, M. Ravilious, A. Kumara-perumal, A. M. Benatamane, M. Galbraith, D. Staton, K. Benoit, and M. Mueller, "1mw multi-stage air-cored permanent magnet generator for wind turbines," in *6th IET International Conference on Power Electronics, Machines and Drives (PEMD 2012)*, 2012, pp. 1–6.
- [21] M. Vatani, A. Mohammadi, D. Lewis, J. F. Eastham, and D. M. Ionel, "Coreless axial flux Halbach array permanent magnet generator concept for direct-drive wind turbine," in *2023 12th International Conference on Renewable Energy Research and Applications (ICRERA)*, 2023, pp. 612–617.
- [22] "Marand Electric Solar Car In-Wheel Motors." [Online]. Available: <https://ia804703.us.archive.org/20/items/pdfy-vz9FEuZlaOhE-jjQ/Solar%20Car%20Wheel%20Motor%20Information%20Sheet.pdf>
- [23] N. Taran, V. Rallabandi, G. Heins, and D. M. Ionel, "Coreless and conventional axial flux permanent magnet motors for solar cars," *IEEE Transactions on Industry Applications*, vol. 54, no. 6, pp. 5907–5917, 2018.
- [24] R. Hill-Cottingham, P. Coles, J. Eastham, F. Profumo, A. Tenconi, and G. Gianolio, "Multi-disc axial flux stratospheric aircraft propeller drive," in *Conference Record of the 2001 IEEE Industry Applications Conference. 36th IAS Annual Meeting (Cat. No.01CH37248)*, vol. 3, 2001, pp. 1634–1639 vol.3.
- [25] M. Vatani, Y. Chulaee, A. Mohammadi, D. R. Stewart, J. F. Eastham, and D. M. Ionel, "On the optimal design of coreless AFPM machines with Halbach array rotors for electric aircraft propulsion," in *IEEE Transportation Electrification Conference & Expo (ITEC)*. IEEE, 2024.
- [26] Y. Chulaee, D. Lewis, A. Mohammadi, G. Heins, D. Patterson, and D. M. Ionel, "Circulating and eddy current losses in coreless axial flux PM machine stators with PCB windings," *IEEE Transactions on Industry Applications*, vol. 59, no. 4, pp. 4010–4020, 2023.
- [27] M. A. Mueller and A. S. McDonald, "A lightweight low-speed permanent magnet electrical generator for direct-drive wind turbines," *Wind Energy: An International Journal for Progress and Applications in Wind Power Conversion Technology*, vol. 12, no. 8, pp. 768–780, 2009.
- [28] O. Keysan, A. S. McDonald, and M. Mueller, "A direct drive permanent magnet generator design for a tidal current turbine(seagen)," in *2011 IEEE International Electric Machines & Drives Conference (IEMDC)*, 2011, pp. 224–229.
- [29] S. Moury and M. T. Iqbal, "A permanent magnet generator with pcb stator for low speed marine current applications," in *2009 1st International Conference on the Developments in Renewable Energy Technology (ICDRET)*. IEEE, 2009, pp. 1–4.
- [30] G. Romeo, G. Frulla, and E. Cestino, "Design of a high-altitude long-endurance solar-powered unmanned air vehicle for multi-payload and operations," *Proceedings of the Institution of Mechanical Engineers, Part G: Journal of Aerospace Engineering*, vol. 221, no. 2, pp. 199–216, 2007.
- [31] E. Cestino, "Design of solar high altitude long endurance aircraft for multi payload & operations," *Aerospace science and technology*, vol. 10, no. 6, pp. 541–550, 2006.
- [32] D. Lawhorn, V. Rallabandi, and D. M. Ionel, "Multi-objective optimization for aircraft power systems using a network graph representation,"

- IEEE Transactions on Transportation Electrification*, vol. 7, no. 4, pp. 3021–3031, 2021.
- [33] M. Vatani, J. F. Eastham, and D. M. Ionel, “Multi-disk coreless axial flux permanent magnet synchronous motors with surface PM and Halbach array rotors for electric aircraft propulsion,” in *2024 IEEE Energy Conversion Congress and Exposition (ECCE)*. IEEE, 2024.
- [34] D. D. Lewis, D. R. Stewart, M. Vatani, O. A. Badewa, A. Mohammadi, and D. M. Ionel, “Fault-tolerant topologies with Halbach array and PM-free multi-stage multi-module electric machines for electric aircraft propulsion,” in *IEEE Energy Conversion Congress & Expo (ECCE)*. IEEE, 2024.
- [35] K. William, “Dynamolectric machine,” US Patent US3 292 024A, Dec., 1966.
- [36] R. L. Fisher, “Ironless armature torque motor,” National Aeronautics and Space Administration, Tech. Rep., Sep. 1972. [Online]. Available: <https://ntrs.nasa.gov/citations/19730013689>
- [37] P. A. Studer, “An ironless armature brushless torque motor,” *Significant Accomplishments in Technol.*, 1972, Jan. 1973. [Online]. Available: <https://ntrs.nasa.gov/citations/19730019098>
- [38] K. R. Pullen, K. J. Horton, M. R. Etemad, A. Fenocchi, L. W. Eggleston, and H. R. Bolton, “Axial field electrical generator,” US Patent US5 021 698A, Jun., 1991.
- [39] K. Pullen, M. Etemad, and A. Fenocchi, “The high speed axial flux disc generator - unlocking the potential of the automotive gas turbine,” *IET Conference Proceedings*, pp. 8–8(1), January 1996. [Online]. Available: https://digital-library.theiet.org/content/conferences/10.1049/ic_19960900
- [40] F. Caricchi, F. Crescimbeni, F. Mezzetti, and E. Santini, “Multistage axial-flux PM machine for wheel direct drive,” *IEEE Transactions on Industry Applications*, vol. 32, no. 4, pp. 882–888, 1996.
- [41] F. Caricchi, F. Crescimbeni, O. Honorati, G. Bianco, and E. Santini, “Performance of coreless-winding axial-flux permanent-magnet generator with power output at 400 Hz, 3000 r/min,” *IEEE Transactions on Industry Applications*, vol. 34, no. 6, pp. 1263–1269, 1998.
- [42] H. Lovatt, V. Ramsden, and B. Mecrow, “Design of an in-wheel motor for a solar-powered electric vehicle,” in *1997 Eighth International Conference on Electrical Machines and Drives (Conf. Publ. No. 444)*, 1997, pp. 234–238.
- [43] V. Ramsden, B. Mecrow, H. Lovatt, and P. Gwan, “A high efficiency in-wheel drive motor for a solar-powered vehicle,” in *IEE Colloquium on Electrical Machine Design for All-Electric and Hybrid-Electric Vehicles (Ref. No. 1999/196)*, 1999, pp. 3/1–3/6.
- [44] N. Lombard and M. Kamper, “Analysis and performance of an ironless stator axial flux PM machine,” *IEEE Transactions on Energy Conversion*, vol. 14, no. 4, pp. 1051–1056, 1999.
- [45] J. Eastham, F. Profumo, A. Tenconi, R. Hill-Cottingham, P. Coles, and G. Gianolio, “Novel axial flux machine for aircraft drive: design and modeling,” *IEEE Transactions on Magnetics*, vol. 38, no. 5, pp. 3003–3005, 2002.
- [46] C. W. Gabrys, “High performance air core motor-generator winding,” US Patent US7 402 934B1, Jul., 2008. [Online]. Available: <https://patents.google.com/patent/US7402934B1/en>
- [47] L. M. Jore and M. B. Jore, “Conductor optimized axial field rotary energy device,” US Patent US7 109 625B1, Sep., 2006.
- [48] M. Awazu and K. Seko, “Axial gap coreless motor and positioning unit,” US Patent US20 080 100 157A1, May, 2008.
- [49] M. B. Jore, L. Jore, M. A. Kvam, J. D. Jore, D. Samsel, J. D. Duford, and J. S. Smith, “Systems and methods for improved direct drive generators,” US Patent US9 154 024B2, Oct., 2015.
- [50] “Launchpoint Technologies 6” Dual Halbach Air-core Motor.” [Online]. Available: <https://www.launchpnt.com/hs-fs/hub/53140/file-14467905-pdf>
- [51] “Motors.” [Online]. Available: <https://launchpointeps.com/motors/>
- [52] *ECM PCB Stator Tech*, <https://pcbstator.com/>, 2024.
- [53] T. J. Woolmer and M. D. McCulloch, “Axial flux permanent magnet machines: A new topology for high performance applications,” in *IET - The Institution of Engineering and Technology Hybrid Vehicle Conference 2006*, 2006, pp. 27–42.
- [54] J. Zhao, X. Liu, S. Wang, and L. Zheng, “Review of Design and Control Optimization of Axial Flux PMSM in Renewable-energy Applications,” *Chinese Journal of Mechanical Engineering*, vol. 36, no. 1, p. 45, Apr. 2023. [Online]. Available: <https://cjme.springeropen.com/articles/10.1186/s10033-023-00868-8>
- [55] N. S., S. P. Nikam, S. Singh, S. Pal, A. K. Wankhede, and B. G. Fernandes, “High-speed coreless axial-flux permanent-magnet motor with printed circuit board winding,” *IEEE Transactions on Industry Applications*, vol. 55, no. 2, pp. 1954–1962, 2019.
- [56] N. S., S. P. Nikam, S. Pal, A. K. Wankhede, and B. G. Fernandes, “Performance comparison between PCB-stator and laminated-core-stator-based designs of axial flux permanent magnet motors for high-speed low-power applications,” *IEEE Transactions on Industrial Electronics*, vol. 67, no. 7, pp. 5269–5277, 2020.
- [57] A. C. Barmpatza and J. C. Kappatou, “Demagnetization faults detection in an axial flux permanent magnet synchronous generator,” in *2017 IEEE 11th International Symposium on Diagnostics for Electrical Machines, Power Electronics and Drives (SDEMPED)*, 2017, pp. 153–159.
- [58] N. Taran, G. Heins, V. Rallabandi, D. Patterson, and D. M. Ionel, “Evaluating the effects of electric and magnetic loading on the performance of single-and double-rotor axial-flux pm machines,” *IEEE Transactions on Industry Applications*, vol. 56, no. 4, pp. 3488–3497, 2020.
- [59] C. Jenkins, S. Jones-Jackson, I. Zaher, G. Pietrini, R. Rodriguez, J. Cotton, and A. Emadi, “Innovations in axial flux permanent magnet motor thermal management for high power density applications,” *IEEE Transactions on Transportation Electrification*, vol. 9, no. 3, pp. 4380–4405, 2023.
- [60] K. Sitapati and R. Krishnan, “Performance comparisons of radial and axial field, permanent-magnet, brushless machines,” *IEEE Transactions on Industry Applications*, vol. 37, no. 5, pp. 1219–1226, 2001.
- [61] A. Ghaheeri, A. Mohammadi Ajamloo, H. Torkaman, and E. Afjei, “Design, modelling and optimisation of a slot-less axial flux permanent magnet generator for direct-drive wind turbine application,” *IET Electric Power Applications*, vol. 14, no. 8, pp. 1327–1338, 2020. [Online]. Available: <https://ietresearch.onlinelibrary.wiley.com/doi/abs/10.1049/iet-epa.2019.0385>
- [62] C. Wang, J. Han, Z. Zhang, Y. Hua, and H. Gao, “Design and optimization analysis of coreless stator axial-flux permanent magnet in-wheel motor for unmanned ground vehicle,” *IEEE Transactions on Transportation Electrification*, vol. 8, no. 1, pp. 1053–1062, 2022.
- [63] F. Marcolini, G. De Donato, F. Giulii Capponi, M. Incurvati, and F. Caricchi, “Design of a multiphase coreless axial flux permanent magnet machine for unmanned aerial vehicle propulsion,” in *2020 IEEE Energy Conversion Congress and Exposition (ECCE)*, 2020, pp. 1756–1763.
- [64] F. Marcolini, G. De Donato, F. G. Capponi, M. Incurvati, and F. Caricchi, “Novel multiphysics design methodology for coreless axial flux permanent magnet machines,” *IEEE Transactions on Industry Applications*, vol. 59, no. 3, pp. 3220–3231, 2023.
- [65] F. Pranjic and P. Vrtic, “Designing rotor disks of a coreless axial flux permanent magnet machines by using simplified fem and an approximation method,” *IEEE Transactions on Energy Conversion*, vol. 35, no. 3, pp. 1505–1512, 2020.
- [66] P. Evans, D. Brown, and J. F. Eastham, “A study of permanent magnet disc motor design,” *BICEM '87, Beijing, China*, pp. 729–732, 1987.
- [67] R. Roy, S. Ramasami, and L. N. Chokkalingam, “Review on thermal behavior and cooling aspects of axial flux permanent magnet motors—a mechanical approach,” *IEEE Access*, vol. 11, pp. 6822–6836, 2023.
- [68] A. S. McDonald, M. Benatmane, and M. A. Mueller, “A multi-stage axial flux permanent magnet machine for direct drive wind turbines,” in *IET Conference on Renewable Power Generation (RPG 2011)*, 2011, pp. 1–6.
- [69] H. Cimen and M. Mueller, “6-rpm 5MW axial flux multi-stage air cored permanent magnet generator design for vertical axis offshore wind turbines,” in *11th International Conference on Power Electronics, Machines and Drives (PEMD 2022)*, vol. 2022. IET, 2022, pp. 395–399.
- [70] A. Habib, H. S. Che, N. Abd Rahim, M. Tousizadeh, and E. Sulaiman, “A fully coreless multi-stator multi-rotor (MSMR) AFPM generator with combination of conventional and Halbach magnet arrays,” *Alexandria Engineering Journal*, vol. 59, no. 2, pp. 589–600, 2020. [Online]. Available: <https://www.sciencedirect.com/science/article/pii/S1110016820300405>
- [71] M. R. Minaz and M. Çelebi, “Design and analysis of a new axial flux coreless PMSG with three rotors and double stators,” *Results in Physics*, vol. 7, pp. 183–188, 2017. [Online]. Available: <https://www.sciencedirect.com/science/article/pii/S2211379716302819>
- [72] A. A. Yusuf, M. Irfan, and M. F. Razzaq, “A design of coreless permanent magnet axial flux generator for low speed wind turbine,” in *2018 5th International Conference on Electrical Engineering, Computer Science and Informatics (EECSI)*, 2018, pp. 637–641.
- [73] S. Javadi and M. Mirsalim, “A coreless axial-flux permanent-magnet generator for automotive applications,” *IEEE Transactions on Magnetics*, vol. 44, no. 12, pp. 4591–4598, 2008.

- [74] D. Ahmed and A. Ahmad, "An optimal design of coreless direct-drive axial flux permanent magnet generator for wind turbine," *Journal of Physics: Conference Series*, vol. 439, no. 1, p. 012039, Jun 2013. [Online]. Available: <https://dx.doi.org/10.1088/1742-6596/439/1/012039>
- [75] M. R. Mínaz and E. Akcan, "An effective method for detection of demagnetization fault in axial flux coreless PMSG with texture-based analysis," *IEEE Access*, vol. 9, pp. 17 438–17 449, 2021.
- [76] H. Asiful, "Performance analysis for single-stage and multi-stage coreless axial flux permanent magnet generator with different rotor structures / Asiful Habib," Master's thesis, Universiti Malaya, Jun. 2020. [Online]. Available: <http://studentsrepo.um.edu.my/14055/>
- [77] B. Kou, C. Huang, X. Zhao, and L. Zhang, "Comparative analysis of coreless multidisc axial flux permanent magnet motors for electric propulsion system," in *2022 IEEE 5th International Electrical and Energy Conference (CIEEC)*, 2022, pp. 3051–3055.
- [78] C. Sezenoglu and A. Balıkcı, "Coreless AFPM pulsed alternator with low internal inductance," *IEEE Transactions on Plasma Science*, vol. 46, no. 8, pp. 3120–3125, 2018.
- [79] V. Rallabandi, N. Taran, D. M. Ionel, and J. F. Eastham, "Coreless multidisc axial flux PM machine with carbon nanotube windings," *IEEE Transactions on Magnetics*, vol. 53, no. 6, pp. 1–4, 2017.
- [80] X. Wang, M. Zhao, Y. Zhou, Z. Wan, and W. Xu, "Design and analysis for multi-disc coreless axial-flux permanent-magnet synchronous machine," *IEEE Transactions on Applied Superconductivity*, vol. 31, no. 8, pp. 1–4, 2021.
- [81] S. Khan, S. S. H. Bukhari, and J.-S. Ro, "Design and analysis of a 4-kw two-stack coreless axial flux permanent magnet synchronous machine for low-speed applications," *IEEE Access*, vol. 7, pp. 173 848–173 854, 2019.
- [82] C. Soneda, H. Asai, Y. Hatta, T. Shimono, and K. Ohnishi, "Design and analysis of core-less multi-layered axial motor," in *2019 IEEE 28th International Symposium on Industrial Electronics (ISIE)*, 2019, pp. 267–272.
- [83] C. Sezenoğlu and A. Balıkcı, "Design of axial flux permanent magnet generator for generator driven electromagnetic launcher," in *2015 9th International Conference on Electrical and Electronics Engineering (ELECO)*, 2015, pp. 595–598.
- [84] X. Wang, M. Zhao, Z. Wan, and W. Xu, "Electromagnetic design of multi-disc coreless axial magnetic flux permanent magnet motor," in *2020 IEEE International Conference on Applied Superconductivity and Electromagnetic Devices (ASEMD)*, 2020, pp. 1–2.
- [85] C. Huang, B. Kou, X. Zhao, X. Niu, and L. Zhang, "Multi-objective optimization design of a stator coreless multidisc axial flux permanent magnet motor," *Energies*, vol. 15, no. 13, 2022. [Online]. Available: <https://www.mdpi.com/1996-1073/15/13/4810>
- [86] X. Wang, M. Zhao, L. Tang, W. Xu, and M. R. Islam, "Fault-tolerant analysis and design of AFPMSM with multi-disc type coreless open-end winding," *IEEE Access*, vol. 8, pp. 171 744–171 753, 2020.
- [87] X. Wang, X. Li, J. Ge, G. Zhang, and W. Xu, "Improved coreless axial flux permanent-magnet machine with nonuniformly distributed winding," *IEEE Transactions on Transportation Electrification*, vol. 9, no. 2, pp. 2557–2567, 2023.
- [88] Q. Zhou and L. Wang, "Simulation and analysis of the fault of coreless axial flux permanent magnet synchronous motor," in *2020 IEEE International Conference on Applied Superconductivity and Electromagnetic Devices (ASEMD)*, 2020, pp. 1–2.
- [89] X. Wang, C. Hu, M. Zhao, L. Wu, and S. Zhou, "Design of multi-layer PCB coreless axial permanent magnet synchronous motor," in *2019 22nd International Conference on Electrical Machines and Systems (ICEMS)*, 2019, pp. 1–4.
- [90] M. J. Kamper, R.-J. Wang, and F. G. Rossouw, "Analysis and performance evaluation of axial flux air-cored stator permanent magnet machine with concentrated coils," in *2007 IEEE International Electric Machines & Drives Conference*, vol. 1, 2007, pp. 13–20.
- [91] M. J. Kamper, R.-J. Wang, and F. G. Rossouw, "Analysis and performance of axial flux permanent-magnet machine with air-cored nonoverlapping concentrated stator windings," *IEEE Transactions on Industry Applications*, vol. 44, no. 5, pp. 1495–1504, 2008.
- [92] N. Taran, V. Rallabandi, and D. M. Ionel, "WAVED: A coreless axial flux PM motor for drive systems with constant power operation," in *2019 IEEE Transportation Electrification Conference and Expo (ITEC)*, 2019, pp. 1–6.
- [93] W.-S. Yao, M.-T. Cheng, and J.-C. Yu, "Novel design of a coreless axial-flux permanent-magnet generator with three-layer winding coil for small wind turbines," *IET Renewable Power Generation*, vol. 14, no. 15, pp. 2924–2932, 2020.
- [94] J. S. Smith, J. D. Duford, J. D. Jore, L. M. Jore, M. B. Jore, and B. J. Sullivan, "Methods and apparatus for overlapping windings," May 27 2014, uS Patent 8,736,133.
- [95] R. L. Kessinger Jr, P. A. Stahura, P. E. Receveur, and K. D. Dockstader, "Interlocking segmented coil array," Apr. 28 1998, uS Patent 5,744,896.
- [96] J. Yang, Y. Gao, J. Chen, C. Zhang, J. Lin, and X. Sun, "Design of axial flux coreless PM motors with the new stator configuration," in *2023 IEEE 18th Conference on Industrial Electronics and Applications (ICIEA)*, 2023, pp. 574–578.
- [97] P. Han, D. Lawhorn, Y. Chulaee, D. Lewis, G. Heins, and D. M. Ionel, "Design optimization and experimental study of coreless axial-flux PM machines with wave winding PCB stators," in *2021 IEEE Energy Conversion Congress and Exposition (ECCE)*, 2021, pp. 4347–4352.
- [98] M. Greaves, B. Guymer, and B. Walsh, "Winding arrangement for an electrical machine," Sep. 2 2014, uS Patent 8,823,238.
- [99] S. Paul, M. Farshadnia, A. Pouramin, J. Fletcher, and J. Chang, "Comparative analysis of wave winding topologies and performance characteristics in ultra-thin printed circuit board axial-flux permanent magnet machine," *IET Electric Power Applications*, vol. 13, no. 5, pp. 694–701, 2019. [Online]. Available: <https://ietresearch.onlinelibrary.wiley.com/doi/abs/10.1049/iet-epa.2018.5417>
- [100] F. Marignetti, G. Volpe, S. M. Mirimani, and C. Cecati, "Electromagnetic design and modeling of a two-phase axial-flux printed circuit board motor," *IEEE Transactions on Industrial Electronics*, vol. 65, no. 1, pp. 67–76, 2018.
- [101] B. Gao, Y. Cheng, Y. Wang, T. Zhao, L. Ding, S. Cui, X. Liu, and Y. Shi, "Optimal design of PCB coreless axial flux permanent magnet synchronous motor with arc windings," *IEEE Transactions on Energy Conversion*, pp. 1–10, 2023.
- [102] S. P. Colyer, P. Arumugam, and J. F. Eastham, "Modular airgap windings for linear permanent magnet machines," *IET Electric Power Applications*, vol. 12, no. 7, pp. 953–961, 2018.
- [103] B. Xia, J.-X. Shen, P. C.-K. Luk, and W. Fei, "Comparative study of air-cored axial-flux permanent-magnet machines with different stator winding configurations," *IEEE Transactions on Industrial Electronics*, vol. 62, no. 2, pp. 846–856, 2015.
- [104] V. Rallabandi, N. Taran, and D. M. Ionel, "Multilayer concentrated windings for axial flux PM machines," in *2016 IEEE Conference on Electromagnetic Field Computation (CEFC)*, 2016, pp. 1–1.
- [105] V. Rallabandi, N. Taran, and D. M. Ionel, "Multilayer concentrated windings for axial flux PM machines," *IEEE Transactions on Magnetics*, vol. 53, no. 6, pp. 1–4, 2017.
- [106] W. Fei, P. C.-K. Luk, and K. Jinupun, "Design and analysis of high-speed coreless axial flux permanent magnet generator with circular magnets and coils," *IET electric power applications*, vol. 4, no. 9, pp. 739–747, 2010.
- [107] W. Fei and P. C. K. Luk, "Design and performance analysis of a high-speed air-cored axial-flux permanent-magnet generator with circular magnets and coils," in *2009 IEEE International Electric Machines and Drives Conference*, 2009, pp. 1617–1624.
- [108] J. Bumby and R. Martin, "Axial-flux permanent-magnet air-cored generator for small-scale wind turbines," *IEE Proceedings-Electric Power Applications*, vol. 152, no. 5, pp. 1065–1075, 2005.
- [109] X. Wang, C. Li, and F. Lou, "Geometry optimize of printed circuit board stator winding in coreless axial field permanent magnet motor," in *2016 IEEE Vehicle Power and Propulsion Conference (VPPC)*, 2016, pp. 1–6.
- [110] C. Li, X. Wang, and H. Lv, "Performance improvement by pattern optimization of PCB winding in coreless axial flux permanent magnet motor," in *2021 IEEE 4th International Electrical and Energy Conference (CIEEC)*, 2021, pp. 1–6.
- [111] C. Wang, Z. Zhang, Y. Liu, W. Geng, and H. Gao, "Effect of slot-pole combination on the electromagnetic performance of ironless stator AFPM machine with concentrated windings," *IEEE Transactions on Energy Conversion*, vol. 35, no. 2, pp. 1098–1109, 2020.
- [112] I. Subotic, C. Gammeter, A. Tüysüz, and J. W. Kolar, "Weight optimization of an axial-flux PM machine for airborne wind turbines," in *2016 IEEE International Conference on Power Electronics, Drives and Energy Systems (PEDES)*, 2016, pp. 1–6.
- [113] F. G. Rossouw, "Analysis and design of axial flux permanent magnet wind generator system for direct battery charging applications," Ph.D. dissertation, Stellenbosch: University of Stellenbosch, 2009.
- [114] I. Subotic, C. Gammeter, A. Tüysüz, and J. W. Kolar, "Weight optimisation of coreless axial-flux permanent magnet machines," *IET Electric Power Applications*, vol. 13, no. 5, pp. 594–603, 2019.
- [115] F. Marcolini, G. D. Donato, F. Giulii Capponi, M. Incurvati, and F. Caricchi, "On winding manufacturing technologies for coreless

- axial-flux permanent-magnet machines,” in *2023 IEEE Workshop on Electrical Machines Design, Control and Diagnosis (WEMDCD)*, 2023, pp. 1–7.
- [116] F. Marcolini, G. De Donato, F. G. Capponi, and F. Caricchi, “Design of a high speed printed circuit board coreless axial flux permanent magnet machine,” in *2021 IEEE Energy Conversion Congress and Exposition (ECCE)*, 2021, pp. 4353–4360.
- [117] O. Taqavi and S. M. Mirimani, “Design aspects, winding arrangements and applications of printed circuit board motors: a comprehensive review,” *IET Electric Power Applications*, vol. 14, no. 9, pp. 1505–1518, 2020.
- [118] M. G. Kesgin, P. Han, N. Taran, D. Lawhorn, D. Lewis, and D. M. Ionel, “Design optimization of coreless axial-flux PM machines with Litz wire and PCB stator windings,” in *2020 IEEE Energy Conversion Congress and Exposition (ECCE)*, 2020, pp. 22–26.
- [119] S. Butterfield, J. Smith, D. Petch, B. Sullivan, P. Smith, and K. Pierce, “Advanced Gearless Drivetrain - Phase I Technical Report,” Boulder Wind Power, Inc., Tech. Rep. DOE/EE0005138-1, Aug. 2012. [Online]. Available: <https://www.osti.gov/biblio/1050994>
- [120] X. Wang, T. Li, P. Gao, and X. Zhao, “Design and loss analysis of axial flux permanent magnet synchronous motor with PCB distributed winding,” in *2021 24th International Conference on Electrical Machines and Systems (ICEMS)*, 2021, pp. 1112–1117.
- [121] F. Tokgöz, G. Çakal, and O. Keysan, “Design and implementation of an optimized printed circuit board axial-flux permanent magnet machine,” in *2020 International Conference on Electrical Machines (ICEM)*, vol. 1, 2020, pp. 111–116.
- [122] D. Lawhorn, P. Han, D. Lewis, Y. Chulaee, and D. M. Ionel, “On the design of coreless permanent magnet machines for electric aircraft propulsion,” in *2021 IEEE Transportation Electrification Conference & Expo (ITEC)*, 2021, pp. 278–283.
- [123] S. R. Shaw, “Structures and methods for thermal management in printed circuit board stators,” Jun. 6 2017, uS Patent 9,673,684.
- [124] N. Salim, S. P. Nikam, S. Pal, A. K. Wankhede, and B. G. Fernandes, “Multiphysics analysis of printed circuit board winding for high-speed axial flux permanent magnet motor,” *IET Electric Power Applications*, vol. 13, no. 6, pp. 805–811, 2019.
- [125] J. Zhao, Y. Wang, T. Ma, X. Liu, and J. Li, “Losses and thermal analysis of an integrated PCB coreless axial flux PMSM with the drive system,” *IEEE Transactions on Industrial Electronics*, vol. 70, no. 11, pp. 11 022–11 032, 2023.
- [126] D. D. Tremelling, “On the design and analysis of a printed circuit board in a high speed surface permanent magnet axial flux machine,” Ph.D. dissertation, UNIVERSITY OF WISCONSIN-MADISON, 2008.
- [127] V. Rallabandi, N. Taran, D. M. Ionel, and J. F. Eastham, “On the feasibility of carbon nanotube windings for electrical machines — case study for a coreless axial flux motor,” in *2016 IEEE Energy Conversion Congress and Exposition (ECCE)*, 2016, pp. 1–7.
- [128] J. Hendershot, J. R. and T. Miller, *Design of Brushless Permanent-Magnet Motors*. Oxford University Press, 04 1995. [Online]. Available: <https://doi.org/10.1093/oso/9780198593898.001.0001>
- [129] M. Vatani, J. F. Eastham, and D. M. Ionel, “Multi-disk coreless axial flux permanent magnet synchronous motors with surface PM and Halbach array rotors for electric aircraft propulsion,” in *IEEE Energy Conversion Congress & Expo (ECCE)*. IEEE, 2024.
- [130] M. Vatani, Y. Chulaee, J. F. Eastham, and D. M. Ionel, “Analytical and fe modeling for the design of coreless axial flux machines with halbach array and surface pm rotors,” in *2024 IEEE Energy Conversion Congress and Exposition (ECCE)*, 2024, pp. 1–7.
- [131] O. Ubani, “Improving the torque density of C-GEN direct drive axial flux air cored permanent magnet generator,” PhD Dissertation, The University of Edinburgh, 2021.
- [132] O. Taqavi, S. Ehsan Abdollahi, and B. Aslani, “Investigations of magnet shape impacts on coreless axial-flux PM machine performances,” in *2021 12th Power Electronics, Drive Systems, and Technologies Conference (PEDSTC)*, 2021, pp. 1–5.
- [133] C. L. Lok, B. Vengadaesvaran, and S. Ramesh, “Implementation of hybrid pattern search–genetic algorithm into optimizing axial-flux permanent magnet coreless generator (afpmg),” *Electrical Engineering*, vol. 99, pp. 751–761, 2017.
- [134] N. Radwan-Praglowska, “Impact of permanent magnets shape and arrangement for selected parameters in coreless axial flux generator,” in *2018 International Symposium on Electrical Machines (SME)*, 2018, pp. 1–6.
- [135] M. Alamdar Yazdi, S. A. Saied, and S. M. Mirimani, “Design and construction of new axial-flux permanent magnet motor,” *IET Electric Power Applications*, vol. 14, no. 12, pp. 2389–2394, 2020.
- [136] F. Zhao, T. A. Lipo, and B.-I. Kwon, “A novel dual-stator axial-flux spoke-type permanent magnet vernier machine for direct-drive applications,” *IEEE Transactions on Magnetics*, vol. 50, no. 11, pp. 1–4, 2014.
- [137] A. Mohammadi, Y. Chulaee, A. M. Cramer, I. G. Boldea, and D. M. Ionel, “Large-scale design optimization of an axial-flux vernier machine with dual stator and spoke pm rotor for ev in-wheel traction,” *IEEE Transactions on Transportation Electrification*, 2024.
- [138] F. Marcolini, G. De Donato, F. G. Capponi, M. Incurvati, M. Schiestl, and F. Caricchi, “Analysis and design of a low-speed, spoke-type coreless axial-flux permanent-magnet motor,” in *2023 IEEE Energy Conversion Congress and Exposition (ECCE)*. IEEE, 2023, pp. 3759–3766.
- [139] M. Aydin and M. Gulec, “A new coreless axial flux interior permanent magnet synchronous motor with sinusoidal rotor segments,” *IEEE Transactions on Magnetics*, vol. 52, no. 7, pp. 1–4, 2016.
- [140] M. Radulescu, S. Breban, and M. Chirca, “Novel topologies of low-speed axial-flux permanent-magnet micro-wind generator,” *Acta Electrotechnica*, vol. 57, no. 3, 2016.
- [141] M. Chirca, S. Breban, C. Oprea, and M. Radulescu, “Analysis of innovative design variations for double-sided coreless-stator axial-flux permanent-magnet generators in micro-wind power applications,” in *2014 International Conference on Electrical Machines (ICEM)*, 2014, pp. 385–389.
- [142] M. Chirca, S. Breban, C. Oprea, and M. M. Radulescu, “Design analysis of a novel double-sided axial-flux permanent-magnet generator for micro-wind power applications,” in *2014 International Conference on Optimization of Electrical and Electronic Equipment (OPTIM)*, 2014, pp. 472–476.
- [143] M. Chirca, S. Breban, C. Oprea, and M. M. Radulescu, “Comparative design analysis of ferrite-permanent-magnet micro-wind turbine generators,” in *2015 Intl Aegean Conference on Electrical Machines & Power Electronics (ACEMP), 2015 Intl Conference on Optimization of Electrical & Electronic Equipment (OPTIM) & 2015 Intl Symposium on Advanced Electromechanical Motion Systems (ELECTROMOTION)*. IEEE, 2015, pp. 687–692.
- [144] M. Chirca, M. M. Radulescu, and C. Rusu, “Design optimization and prototyping of a double-rotor axial-flux spoke-type ferrite-magnet micro-wind generator,” in *2021 International Aegean Conference on Electrical Machines and Power Electronics (ACEMP) & 2021 International Conference on Optimization of Electrical and Electronic Equipment (OPTIM)*. IEEE, 2021, pp. 8–13.
- [145] J. Mallinson, “One-sided fluxes – a magnetic curiosity?” *IEEE Transactions on Magnetics*, vol. 9, no. 4, pp. 678–682, 1973.
- [146] K. Halbach, “Design of permanent multipole magnets with oriented rare earth cobalt material,” *Nuclear Instruments and Methods*, vol. 169, no. 1, pp. 1–10, 1980.
- [147] K. Halbach, “Physical and optical properties of rare earth cobalt magnets,” *Nuclear Instruments and Methods in Physics Research*, vol. 187, no. 1, pp. 109–117, 1981.
- [148] Y. Chulaee, D. Lewis, M. Vatani, J. F. Eastham, and D. M. Ionel, “Torque and power capabilities of coreless axial flux machines with surface PMs and Halbach array rotors,” in *2023 IEEE International Electric Machines & Drives Conference (IEMDC)*, San Francisco, CA. IEEE, 2023, pp. 1–6.
- [149] M. Vatani, Y. Chulaee, J. F. Eastham, X. Pei, and D. M. Ionel, “Multi-wound axial flux generators with halbach array rotors,” in *2024 IEEE Energy Conversion Congress and Exposition (ECCE)*, 2024, pp. 1–6.
- [150] G. Ramian, L. Elias, and I. Kimel, “Micro-undulator FELS,” *Nuclear Instruments and Methods in Physics Research Section A: Accelerators, Spectrometers, Detectors and Associated Equipment*, vol. 250, no. 1–2, pp. 125–133, 1986.
- [151] W. S. P. Robertson, “Modelling and design of magnetic levitation systems for vibration isolation.” Ph.D. dissertation, University of Adelaide, 2013.
- [152] O. G. Ubani, M. A. Mueller, J. Chick, and A. McDonald, “Analysis of an air-cored axial flux permanent magnet machine with Halbach array,” in *8th IET International Conference on Power Electronics, Machines and Drives (PEMD 2016)*, 2016, pp. 1–6.
- [153] M. Galea, “High performance, direct drive machines for aerospace applications,” Ph.D. dissertation, University of Nottingham, 2013.
- [154] Y. Chulaee, D. Lewis, M. Vatani, J. F. Eastham, and D. M. Ionel, “Torque and power capabilities of coreless axial flux machines with surface PMs and Halbach array rotors,” in *2023 IEEE International Electric Machines & Drives Conference (IEMDC)*, 2023, pp. 1–6.
- [155] Y. Shen, G. Liu, Z. Xia, and Z.-Q. Zhu, “Determination of maximum electromagnetic torque in pm brushless machines having two-segment

- Halbach array," *IEEE Transactions on Industrial Electronics*, vol. 61, no. 2, pp. 718–729, 2013.
- [156] M. R. Ricci, J. G. Sugar, B. E. Paden, and D. B. Paden, "Axial flux brushless permanent magnet electrical machine rotor," Nov. 27 2018, uS Patent 10,141,822.
- [157] M. R. Ricci, J. G. Sugar, B. E. Paden, and D. B. Paden, "Axial flux brushless permanent magnet electrical machine rotor," Nov. 5 2019, uS Patent 10,468,955.
- [158] M. R. Ricci, D. B. Paden, V. Varahamurthy, B. J. Clark, and B. E. Paden, "Lightweight, high-efficiency, energy-dense, hybrid power system for reliable electric flight," Aug. 29 2023, uS Patent 11,738,875.
- [159] G. A. Long, B. E. Paden, M. R. Ricci, D. B. Paden, and J. G. Sugar, "Lightweight and efficient electrical machine and method of manufacture," Feb. 25 2020, uS Patent 10,574,110.
- [160] K. P. Duffy, "Optimizing power density and efficiency of a double-Halbach permanent-magnet ironless axial flux motor," in *52nd AIAA/SAE/ASEE Joint Propulsion Conference*, 2016, p. 4712.
- [161] T. F. Talerico, J. C. Chin, and Z. A. Cameron, "Optimization of an air core dual Halbach array axial flux rim drive for electric aircraft," in *AIAA Aviation Forum*, no. GRC-E-DAA-TN56733, 2018.
- [162] S. Gair, A. Canova, J. Eastham, and T. Betzer, "A new 2d FEM analysis of a disc machine with offset rotor," in *Proceedings of International Conference on Power Electronics, Drives and Energy Systems for Industrial Growth*, vol. 1, 1996, pp. 617–621 vol.1.
- [163] M. Gulec and M. Aydin, "Implementation of different 2D finite element modelling approaches in axial flux permanent magnet disc machines," *IET Electric Power Applications*, vol. 12, no. 2, pp. 195–202, 2018.
- [164] J. R. Bumby, R. Martin, M. Mueller, E. Spooner, N. Brown, and B. Chalmers, "Electromagnetic design of axial-flux permanent magnet machines," *IEE Proceedings-Electric Power Applications*, vol. 151, no. 2, pp. 151–160, 2004.
- [165] P. Virtic, P. Pisek, T. Marcic, M. Hadziselimovic, and B. Stumberger, "Analytical analysis of magnetic field and back electromotive force calculation of an axial-flux permanent magnet synchronous generator with coreless stator," *IEEE Transactions on Magnetics*, vol. 44, no. 11, pp. 4333–4336, 2008.
- [166] T. F. Chan, L. L. Lai, and S. Xie, "Field computation for an axial flux permanent-magnet synchronous generator," *IEEE Transactions on Energy Conversion*, vol. 24, no. 1, pp. 1–11, 2009.
- [167] J.-Y. Choi, S.-H. Lee, K.-J. Ko, and S.-M. Jang, "Improved analytical model for electromagnetic analysis of axial flux machines with double-sided permanent magnet rotor and coreless stator windings," *IEEE Transactions on Magnetics*, vol. 47, no. 10, pp. 2760–2763, 2011.
- [168] Z. Frank and J. Laksar, "Analytical design of coreless axial-flux permanent magnet machine with planar coils," *IEEE Transactions on Energy Conversion*, vol. 36, no. 3, pp. 2348–2357, 2021.
- [169] D. M. Ionel and M. Popescu, "Finite-element surrogate model for electric machines with revolving field—application to iPM motors," *IEEE Transactions on Industry Applications*, vol. 46, no. 6, pp. 2424–2433, 2010.
- [170] D. M. Ionel and M. Popescu, "Ultra-fast finite element analysis of brushless PM machines based on space-time transformations," in *2009 IEEE International Electric Machines and Drives Conference*, 2009, pp. 521–528.
- [171] Y. Chulaae and D. M. Ionel, "Ultra-fast finite element analysis of coreless axial flux permanent magnet synchronous machines," *IET Electric Power Applications*, 2024. [Online]. Available: <https://ietresearch.onlinelibrary.wiley.com/doi/abs/10.1049/elp2.12439>
- [172] Y. Zhilichev, "Three-dimensional analytic model of permanent magnet axial flux machine," *IEEE Transactions on Magnetics*, vol. 34, no. 6, pp. 3897–3901, 1998.
- [173] O. de la Barriere, S. Hlioui, H. Ben Ahmed, M. Gabsi, and M. LoBue, "3-D formal resolution of Maxwell equations for the computation of the no-load flux in an axial flux permanent-magnet synchronous machine," *IEEE Transactions on Magnetics*, vol. 48, no. 1, pp. 128–136, 2012.
- [174] S. G. Min and B. Sarlioglu, "3-d performance analysis and multiobjective optimization of coreless-type pm linear synchronous motors," *IEEE Transactions on Industrial Electronics*, vol. 65, no. 2, pp. 1855–1864, 2017.
- [175] W. K. Thompson, "Three-dimensional field solutions for multi-pole cylindrical Halbach arrays in an axial orientation," National Aeronautics and Space Administration, Tech. Rep., 2006.
- [176] A. Mohammadpour, A. Gandhi, and L. Parsa, "Winding factor calculation for analysis of back emf waveform in air-core permanent magnet linear synchronous motors," *IET Electric Power Applications*, vol. 6, no. 5, pp. 253–259, 2012.
- [177] S. Mohammadi and M. Mirsalim, "Analytical design framework for torque and back-emf optimization, and inductance calculation in double-rotor radial-flux air-cored permanent-magnet synchronous machines," *IEEE Transactions on Magnetics*, vol. 50, no. 1, pp. 1–16, 2014.
- [178] Y. Zhang, Y. Wang, and S. Gao, "3-d magnetic equivalent circuit model for a coreless axial flux permanent-magnet synchronous generator," *IET Electric Power Applications*, vol. 15, no. 10, pp. 1261–1273, 2021.
- [179] J. Zhao, T. Ma, X. Liu, G. Zhao, and N. Dong, "Performance analysis of a coreless axial-flux PMSM by an improved magnetic equivalent circuit model," *IEEE Transactions on Energy Conversion*, vol. 36, no. 3, pp. 2120–2130, 2021.
- [180] X. Ding, G. Liu, M. Du, H. Guo, H. Qian, and C. Gerada, "Development of an axial flux MEMS BLDC micromotor with increased efficiency and power density," *Energies*, vol. 8, no. 7, pp. 6608–6626, 2015.
- [181] M. Aydin, M. Gulec, Y. Demir, B. Akyuz, and E. Yolacan, "Design and validation of a 24-pole coreless axial flux permanent magnet motor for a solar powered vehicle," in *2016 XXII International Conference on Electrical Machines (ICEM)*, 2016, pp. 1493–1498.
- [182] A. Daghigh, H. Javadi, and H. Torkaman, "Design optimization of direct-coupled ironless axial flux permanent magnet synchronous wind generator with low cost and high annual energy yield," *IEEE Transactions on Magnetics*, vol. 52, no. 9, pp. 1–11, 2016.
- [183] R.-J. Wang and M. Kamper, "Calculation of eddy current loss in axial field permanent-magnet machine with coreless stator," *IEEE Transactions on Energy Conversion*, vol. 19, no. 3, pp. 532–538, 2004.
- [184] A. Ahfock and D. Gambetta, "Stator eddy-current losses in printed circuit brushless motors," *IET electric power applications*, vol. 5, no. 1, pp. 159–167, 2011.
- [185] N. Taran, D. M. Ionel, V. Rallabandi, G. Heins, and D. Patterson, "An overview of methods and a new three-dimensional FEA and analytical hybrid technique for calculating AC winding losses in PM machines," *IEEE Transactions on Industry Applications*, vol. 57, no. 1, pp. 352–362, 2021.
- [186] L. Yang, J. Zhao, W. Fu, X. Liu, J. Zhu, and C. Ai, "A comprehensive investigation of winding eddy and circulating current losses of stator iron coreless PMBLDC motors," *Energies*, vol. 16, no. 14, p. 5523, 2023.
- [187] J. Santiago, J. G. Oliveira, J. Lundin, A. Larsson, and H. Bernhoff, "Losses in axial-flux permanent-magnet coreless flywheel energy storage systems," in *2008 18th International Conference on Electrical Machines*, 2008, pp. 1–5.
- [188] G. François and B. Dehez, "Impact of slit configuration on eddy current and supply current losses in PCB winding of slotless PM machines," *IEEE Transactions on Industry Applications*, vol. 58, no. 5, pp. 6035–6044, 2022.
- [189] D. Talebi, M. C. Gardner, S. V. Sankarraman, A. Daniar, and H. A. Toliyat, "Electromagnetic design characterization of a dual rotor axial flux motor for electric aircraft," *IEEE Transactions on Industry Applications*, vol. 58, no. 6, pp. 7088–7098, 2022.
- [190] J. Wang, K. Atallah, R. Chin, W. M. Arshad, and H. Lendenmann, "Rotor eddy-current loss in permanent-magnet brushless AC machines," *IEEE Transactions on Magnetics*, vol. 46, no. 7, pp. 2701–2707, 2010.
- [191] W. H. Hayt and J. A. Buck, *Engineering electromagnetics*, 8th ed. New York, NY: McGraw-Hill, 2012.
- [192] M. Rosu, P. Zhou, D. Lin, D. M. Ionel, M. Popescu, F. Blaabjerg, V. Rallabandi, and D. Staton, *Multiphysics simulation by design for electrical machines, power electronics and drives*. John Wiley & Sons, 2017.
- [193] Z. S. Du and J. Tangudu, "Novel compact 3-D PM machines for ultra high power density applications," in *2023 IEEE International Electric Machines & Drives Conference (IEMDC)*. IEEE, 2023, pp. 1–7.
- [194] PCB Stator, "Applications of pcb stator technology," <https://pcbstator.com/applications/>, n.d.
- [195] V. Rallabandi, D. Lawhorn, J. He, and D. M. Ionel, "Current weakening control of coreless afpm motor drives for solar race cars with a three-port bi-directional dc/dc converter," in *2017 IEEE 6th International Conference on Renewable Energy Research and Applications (ICR-ERA)*. IEEE, 2017, pp. 739–744.
- [196] K. S. Haran, S. Kalsi, T. Arndt, H. Karmaker, R. Badcock, B. Buckley, T. Haugan, M. Izumi, D. Loder, J. W. Bray *et al.*, "High power density superconducting rotating machines—development status and technology roadmap," *Superconductor Science and Technology*, vol. 30, no. 12, p. 123002, 2017.

- [197] J. Sun, J. Zheng, Y. Song, L. Wang, X. Liu, and X. Ni, "Design of axial flux HTS machine prototype and AC losses calculation," *IEEE Transactions on Applied Superconductivity*, 2023.
- [198] R. Berger, "Hydrogen: A future fuel for aviation," 2024. [Online]. Available: <https://www.rolandberger.com/en/Insights/Publications/Hydrogen-A-future-fuel-for-aviation.html>
- [199] Advanced Research Projects Agency - Energy (ARPA-E). (n.d.) ARPA-E: ASCEND program. [Online]. Available: <https://arpa-e.energy.gov/technologies/programs/ascend>
- [200] NASA Techport. (2024) Integrated zero-emission aviation (izea) using a robust hybrid architecture. [Online]. Available: <https://techport.nasa.gov/view/106525>
- [201] ARPA-E, "Multi-physical co-design of next generation axial motors for aerospace applications," 2022. [Online]. Available: <https://arpa-e.energy.gov/sites/default/files/2022-07/2022%20Program%20Review%20Slides.pdf>
- [202] K. Saviers, R. Regan, W. Zhao, A. Kuczek, A. Alahyari, Z. S. Du, J. A. Weibel, and J. Tangudu, "Stator prototype for a high current density electric motor: Assembly, evaluation, and testing," in *2023 IEEE Energy Conversion Congress and Exposition (ECCE)*. IEEE, 2023, pp. 1802–1808.
- [203] ARPA-E, "Ultra-light, integrated, reliable, aviation-class co-optimized motor and power converter with advanced cooling technology (ultra-compact)," 2024. [Online]. Available: https://arpa-e.energy.gov/sites/default/files/2024-05/10_ARPA-E_ASCEND_ULTRA-COMPACT_Apr2024_RTRC_0.pdf
- [204] ARPA-E, "2022 reeach/ascend annual review meetings," 2022. [Online]. Available: <https://arpa-e.energy.gov/2022-reeach-ascend-annual-review-meetings>
- [205] ARPA-E, "High power density dual-rotor permanent magnet motor with integrated cooling and drive for aircraft propulsion," 2024. [Online]. Available: https://arpa-e.energy.gov/sites/default/files/2024-05/13_ASCEND_AML_FSU_Annual_Meeting_Presentation_2024.pdf
- [206] C. D. Manolopoulos, M. F. Iacchetti, A. C. Smith, P. Miller, and M. Husband, "Litz wire loss performance and optimization for cryogenic windings," *IET Electric Power Applications*, vol. 17, no. 4, pp. 487–498, 2023.



Martin Vatani (Graduate Student Member, IEEE) received his M.Sc. degree in Electrical Engineering, with a focus on Power Electronics and Electrical Machines, from Amirkabir University of Technology (Tehran Polytechnic), Tehran, Iran, in 2020. He is currently pursuing a Ph.D. in Electrical and Computer Engineering at the University of Kentucky, where he is a graduate research assistant in the SPARK Laboratory. His work is supported by NASA, NSF, and industry-funded projects. His research has been recognized with multiple academic

honors and awards for papers and experimental demonstrations. His research interests include advanced electromagnetic finite element analysis (FEA), electric machine design optimization, and power electronic drives.



Donovin D. Lewis (Graduate Student Member, IEEE) received the B.Sc. degree in electrical engineering in 2021 from the University of Kentucky (UKY), Lexington, KY, USA, where he is working towards the Ph.D. degree with the SPARK Laboratory, Department of Electrical and Computer Engineering as a National Science Foundation (NSF) Graduate Research Fellow and Lighthouse Beacon Foundation Graduate Research Fellow. He also received the Otis A. Singletary Graduate Fellowship at UKY, and paper and student demonstration awards

at IEEE international conferences. Mr. Lewis is also a remote research collaborator with the Oak Ridge National Laboratory, and a summer visitor with the University of Oxford, Oxford, England. His research interests include design and development of wireless charging systems and electric motors.



John Frederic Eastham received the BSc, MSc, Ph.D., and D.Sc. degrees from University of Manchester, U.K. He was a Reader with Imperial College in London, Professor with Aberdeen University, and then Professor and Head of Department at University of Bath, U.K., where he subsequently served as Dean and Pro Vice Chancellor, and is currently Emeritus Professor.

Professor Eastham does much of his work with industry. He was a main board Director of the Mycalex Group Company and a member of the UK Technology Strategy Board. He has worked as a consultant for many companies including Goodrich Aerospace, Force Engineering Ltd, Vestas Wind Systems Ltd and General Electric Global Research. He is the author or co-author of more than 45 patents and 200 technical papers. His public committee work has included chairmanship of the UK Science and Engineering Research Council Electrical Engineering Committee, and membership of the Council for National Academic Awards in the U.K.

Professor Eastham is a Fellow of the Royal Society of Edinburgh, of the Royal Academy of Engineering, and of the Institution of Engineering and Technology (IET) in the U.K. He received a Doctorate Honoris Causa from Bucharest University, Romania, and was appointed Honorary Professor by Harbin University and CUMT University in China. He was awarded the Institution of Electrical Engineers Achievement Medal in the Science, Education and Technology Division, and is a recipient of the Powergen Partnership Award, and of the Lifetime Contribution to Magnetics Award from the UK Magnetics Society.



Dan M. Ionel (Fellow, IEEE) received both the M.Eng. and Ph.D. degrees in electrical engineering from the Polytechnic University of Bucharest, Bucharest, Romania. His doctoral studies included a Leverhulme Visiting Fellowship with the University of Bath, Bath, U.K. He was a Postdoctoral Researcher with the SPEED Laboratory, University of Glasgow, Glasgow, U.K.

Previously to 2015, he worked in industry, most recently as Chief Engineer with Regal Beloit Corp., Grafton, WI, USA, and before that as Chief Scientist with Vestas Wind Turbines. He was also a Visiting Professor and a Research Professor with the University of Wisconsin and Marquette University, Milwaukee, WI, USA. He is currently Professor and the L. Stanley Pigman Chair in Power with the University of Kentucky, Lexington, KY, USA, where he is also the Director of the Power and Energy Institute of Kentucky and of the SPARK Laboratory. During his 2024 sabbatical in England, U.K., he was a Leverhulme Visiting Professor with University of Bath, expanding also the collaboration with University of Oxford, and was appointed as an Honorary Professor at University College London (UCL).

Dr. Ionel has contributed to technological developments with long-lasting industrial impact, designed electric machines and drives with ratings between 0.002 and 10,000hp. He holds more than 40 patents, and has authored or coauthored two books and more than 300 technical papers, including IEEE award winners. He served as chair of large committees and conferences for the IEEE power societies, and editor of journals. Dr. Ionel received the Cyril G. Veinott Award, the highest distinction for electromechanical energy conversion contributions from the IEEE PES.